TRIUMF

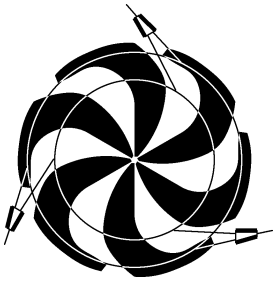

ANNUAL REPORT
SCIENTIFIC ACTIVITIES
1998

CANADA'S NATIONAL MESON FACILITY
OPERATED AS A JOINT VENTURE BY:

MEMBERS:

UNIVERSITY OF ALBERTA
SIMON FRASER UNIVERSITY
UNIVERSITY OF VICTORIA
UNIVERSITY OF BRITISH COLUMBIA

ASSOCIATE MEMBERS:

UNIVERSITY OF MANITOBA
UNIVERSITÉ DE MONTRÉAL
UNIVERSITY OF TORONTO
UNIVERSITY OF REGINA
CARLETON UNIVERSITY
QUEEN'S UNIVERSITY

UNDER A CONTRIBUTION FROM THE
NATIONAL RESEARCH COUNCIL OF CANADA

APRIL 1999

The contributions on individual experiments in this report are outlines intended to demonstrate the extent of scientific activity at TRIUMF during the past year. The outlines are not publications and often contain preliminary results not intended, or not yet ready, for publication. Material from these reports should not be reproduced or quoted without permission from the authors.

Experiment 497
Measurement of the flavour conserving hadronic weak interaction
(J. Birchall, S.A. Page, W.T.H. van Oers, Manitoba)

The ongoing parity violation experiment at TRIUMF will determine the parity-violating longitudinal analyzing power $A_z = (\sigma^+ - \sigma^-)/(\sigma^+ + \sigma^-)$ in $p-p$ elastic scattering at 221 MeV, where σ^+ and σ^- are the scattering cross sections for positive and negative helicity.

The 221 MeV energy of Expt. 497 is chosen so that the measured A_z, accounting for the finite acceptance of the detectors, arises exclusively from the ${}^3P_2$–${}^1D_2$ parity mixed partial wave. (At this energy the contribution to A_z from the ${}^1D_2$–${}^3F_2$ partial wave is only 5% of that from ${}^3P_2$–${}^1D_2$.) The ability to measure at this energy is an advantage of the TRIUMF measurement, as it simplifies the interpretation of the result. For example, if A_z is calculated using a meson exchange model with ρ and ω exchange, then the TRIUMF experiment is sensitive only to the effects of ρ exchange [Simonius, Can. J. Phys. **66**, 548 (1988)] and can be used to extract the weak ρ-meson-nucleon-nucleon coupling constant. In the context of the weak meson exchange model [Desplanques *et al.*, Ann. Phys. (N.Y.) **124**, 449 (1980)], the proposed measurement of A_z to $\pm 0.2 \times 10^{-7}$ will provide a $\pm 25\%$ determination of the weak ρ-nucleon coupling constant $h_\rho^{pp} = (h_\rho^0 + h_\rho^1 + h_\rho^2/\sqrt{6})$.

A major effort to minimize and understand systematic error contributions is required to successfully perform an experiment to this level of precision. The first significant data set for Expt. 497 was acquired in February, 1997, with a raw statistical error of $\pm 0.4 \times 10^{-7}$ and most systematic errors at or below the 10^{-7} level. That result represented a major milestone for the experiment, the culmination of many years of effort to reduce both the helicity correlated beam modulations and the sensitivities to them. The February, 1997 data set is fully described in Araz Hamian's Ph.D. thesis [Hamian, *The measurement of parity violation in proton-proton scattering at 221 MeV*, Ph.D. thesis (University of Manitoba, 1998)].

Beam line and instrumentation

In addition to the measuring apparatus, the optically pumped polarized ion source (OPPIS), cyclotron, and transport beam lines are critical components of the experimental set-up, as illustrated in Fig. 1. A 5 μA transversely polarized beam is transported to the

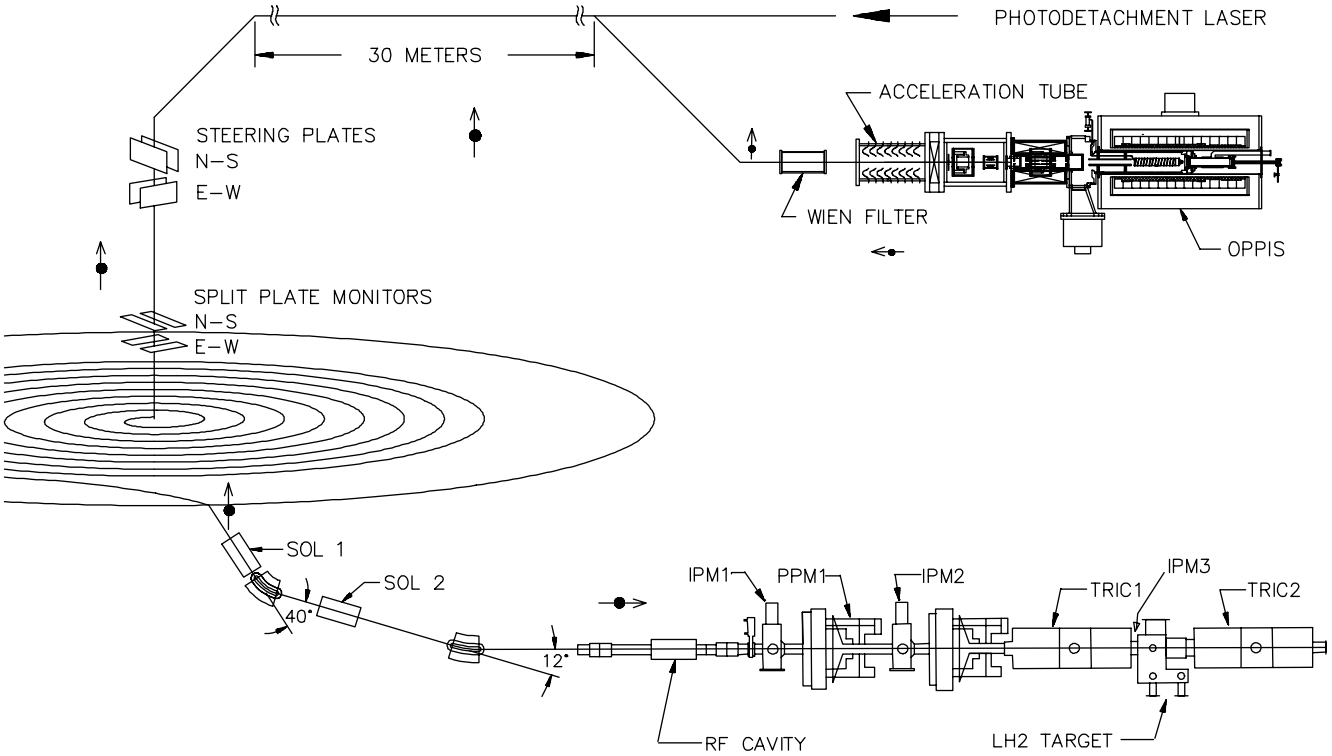

Fig. 1. General layout of the TRIUMF parity experiment. (OPPIS: optically pumped polarized ion source; SOL: spin precession solenoid; IPM: intensity profile monitor; PPM: polarization profile monitor; TRIC: transverse field ionization chamber.)

cyclotron through an approximately 50 m long injection beam line. The ion source Wien filter is tuned to produce vertical polarization at the entrance to the cyclotron. A 200 nA beam at 75–80% vertical polarization is extracted at 221 MeV. Spin precession through a pair of solenoid and dipole magnets results in delivery of a longitudinally polarized beam to the 40 cm liquid hydrogen target, which scatters 4% of the beam. Transverse field parallel plate ion chambers TRIC1 and TRIC2 measure the beam current incident on and transmitted through the target. The parity violation signal is derived from the helicity-correlated difference between the beam currents measured by the two TRICs. Upstream of the target are two polarization profile monitors (PPMs) to measure the distributions of transverse polarization $P_y(x)$ and $P_x(y)$ across the beam, and two intensity profile monitors (IPMs) to measure the intensity distribution of beam current in x and y. The IPMs are coupled to a pair of servo magnets which lock the beam path on the optimum axis through the equipment.

Target upgrade

To correct marginal cooling power experienced during 1996 and 1997, two new CTI cryogenerator units were added at the end of 1997. This upgrade was very successful and the runs in 1998 enjoyed excellent target performance with approximately 15 W of excess cooling power.

Data

The full parity data set now consists of three major (1 month) data runs, taken in February–March, 1997, in December–January, 1998, and July–August, 1998, plus a short run (1 week) taken in August, 1997. The long runs have a raw statistical error of approximately $\pm 0.4 \times 10^{-7}$ each, while the short August, 1997 run has a raw statistical error of $\pm 1 \times 10^{-7}$. Systematic error corrections, however, limit the final precision of the overall result in all cases. A major effort has been under way to analyze these data sets; very significant progress made recently which sheds new light on the dominant systematic error contribution is discussed below.

Data analysis

Every 200 ms, the longitudinal analyzing power A_z is deduced from an 8-state data cycle with spin sequence $(+--+-++-)$ or its complement. The width of the A_z distribution is determined mainly by detector noise and random beam and cyclotron instabilities (the normal 'counting statistics' contribution is negligible). Random noise is minimized by aligning the beam along the symmetry or 'neutral axis' of the apparatus and ensuring that the two TRICs are as identical as possible in their response to the beam. The mean of the A_z distribution can be displaced from zero either by real parity violation or by a false signal from other helicity-correlated changes in beam properties. These false signals are studied in a series of calibration measurements in which small spin-state-correlated modulations of beam current, energy, position, angle, and transverse polarization are purposely introduced. Interspersed data acquired in the frequent spin-off cycles provide an important zero asymmetry check of the apparatus and electronics.

February, 1997 data re-analysis

A thorough re-analysis of the February, 1997 data has recently been completed [Hamian, *op. cit.*], leading to revised conclusions regarding the systematic data offset and sensitivity to polarization moments, the two largest corrections to the data.

In correcting for the effects of transverse polarization we consider **intrinsic** moments of transverse polarization $\langle xP_y \rangle$ and $\langle yP_x \rangle$ resulting from a non-uniform distribution of transverse polarization within the beam envelope, as distinct from the corresponding **extrinsic** polarization moments $\langle x \rangle \langle P_y \rangle$ and $\langle y \rangle \langle P_x \rangle$ which arise when a beam with finite transverse polarization is displaced from the polarization neutral axis. The polarization neutral axis, which defines $\langle x \rangle = 0$, $\langle y \rangle = 0$, is determined from routine calibration scans of the sensitivity to **extrinsic** polarization moments, several times per data run. These scans yield a set of coefficients which are used to correct the raw asymmetries for non-zero average polarization components $\langle P_y \rangle$ and $\langle P_x \rangle$. These extrinsic calibration coefficients also determine the optimum beam convergence at the LH_2 target to minimize the sensitivity to **intrinsic** polarization moments $\langle xP_y \rangle$ and $\langle yP_x \rangle$, as described in previous reports.

It is important to emphasize that the sensitivities of the apparatus to both intrinsic and extrinsic polarization moments should be identical, so that in principle only the extrinsic polarization scans are required to determine the sensitivity coefficients for both effects. However, the distribution of corrected A_z is much broader than that of the raw A_z measurements when the extrinsic coefficients are combined with the intrinsic moments at each PPM to correct the data, since the resolution of the PPMs is significant compared to the intrinsic polarization moments that they measure. For this reason, previous analyses instead relied on a regression analysis to determine the sensitivity to intrinsic moments from correlations of the measured A_z values with the intrinsic first moments.

During the re-analysis of the 1997 data it was discovered that the regression analysis program had been systematically underestimating the sensitivity to intrinsic first moments of transverse polarization. This

was due to the small size of the intrinsic polarization moments relative to the measurement resolution for small data samples. When the data are bundled into samples of 5000 or more event pairs (approx. 1/2 hour acquisition time), the intrinsic moment sensitivities obtained from the regression analysis are in agreement with the sensitivities obtained from the extrinsic coefficients scaled by the average ratio of intrinsic first moments measured by PPM1 and PPM2. It hence seems clear that the sensitivites extracted from the re-analysis are the correct ones.

In examining the problem of the increased noise in the corrected data using the extrinsic polarization moments sensitivities at each PPM, it was realized that corrections for intrinsic polarization moments could be made to greater precision by combining the extrinsic correction coefficients with measurements of the **ratio** of intrinsic moments at PPM1 and PPM2, i.e. $\langle xP_y\rangle_2/\langle xP_y\rangle_1$ and similarly for $\langle yP_x\rangle$, averaged over the entire parity data sample. This reduces the uncertainty in the overall correction, provided that the ratio is consistent over the data sample it is calculated from. This latter requirement implies extremely stable and reproducible beam tune conditions are needed over the course of a 4 week data run, which can be verified by independent measurements with the parity IPMs and other beam line diagnostic monitors. The uncertainty in the overall correction using this method is reduced because the effective sensitivity obtained by scaling the extrinsic correction coefficients by the average intrinsic moments ratio is significantly smaller than the sensitivity at each PPM. If the cyclotron and beam line tune produce precisely the right ratio of intrinsic moments at PPM1 and PPM2, the effective sensitivity to intrinsic moments vanishes.

The results of the re-analysis of the February, 1997 data are shown in Fig. 2. The upper figure shows the data corrected based on extrinsic sensitivity coefficients for transverse polarization moments at each PPM. The lower figure shows the data corrected based on intrinsic polarization moment sensitivities deduced from the regression analysis of the raw A_z data. The corrected A_z values are consistent in both cases; the spread in the data is dramatically reduced using the latter technique. Note that the regression analysis approach requires that the beam tune be constant over the entire set of runs, since it assumes a constant net intrinsic first moment sensitivity, while the approach based on extrinsic coefficients alone is beam tune independent. In any case, there is only one significant correction to the data, corresponding to the intrinsic first moment of transverse polarization $\langle xP_y\rangle$. The corrected A_z values have a reduced χ^2 of 0.5 per degree of freedom, as compared with 10.8 for the raw A_z values

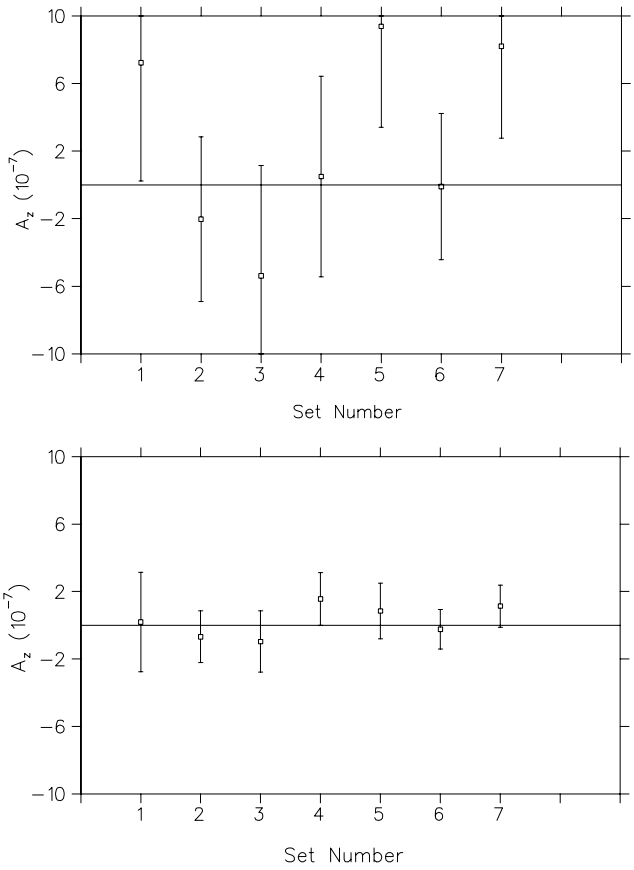

Fig. 2. Corrected A_z from February, 1997 re-analysis. The data are grouped into 7 sets with different relative orientations of the spin in the cyclotron and the parity beam line. The upper figure shows the data corrected based on the extrinsic sensitivity coefficients for transverse polarization moments at each PPM. The lower figure shows the data corrected based on intrinsic moment sensitivities deduced from the regression analysis of the raw A_z data. The corrected A_z values are consistent in both cases; the spread in the data is dramatically reduced using the latter technique.

for the same 7 data sets.

The excellent consistency of the February, 1997 data sets after correcting for all known effects indicates that unmeasured systematic errors correlated with both the direction of spin at the ion source and the direction of spin in the cyclotron are consistent with zero at the level of precision in A_z, approximately $\pm 0.7 \times 10^{-7}$. Thus, the apparent systematic offset associated with the direction of spin in the cyclotron reported in the preliminary analysis of this data set has been shown to be explained by an underestimated sensitivity to the intrinsic polarization moment $\langle xP_y\rangle$. This is a very encouraging result for future work.

The final corrected result from the February, 1997 data set is found to be:

$$A_z = (0.33 \pm 0.57 \pm 0.31) \times 10^{-7} = (0.33 \pm 0.65) \times 10^{-7}$$

where the first error is derived from the standard de-

viation of the corrected A_z distribution ("statistical") and the second is the contribution from the uncertainties in the sensitivity coefficients ("systematic"). The statistical error includes the uncertainty in ΔA_z due to the spread of the helicity correlated beam property measurements, but is dominated by the spread of the raw A_z values. The systematic error, since it is due almost entirely to the uncertainty in the $\langle xP_y \rangle$ sensitivity as determined from the regression analysis of the parity data, is in fact statistics dominated.

August, 1997 data

These data were acquired in two main sets, one in each of the beam line helicity configurations. Unfortunately, much of the running period was lost to technical problems, and the statistical uncertainty is $\pm 1.0 \times 10^{-7}$ for approximately 20 hours of polarized data. This uncertainty will be further increased by corrections for systematic error, giving this data set little weight.

December, 1997 – January, 1998 data

During the December, 1997 – January, 1998 running period, approximately 150 hours of polarized data were acquired in addition to systematic error calibrations and other tests. Although the liquid hydrogen target performed excellently, a failure of the HE2 probe control mechanism prevented the August, 1997 cyclotron tune from being re-established with the ultrathin stripping foil. The thin foil was used for the first half of the run, with the holder shadowed with the beam line 1 extraction foil instead of HE2, but the arrangement was not optimal, and a great deal of extra time was spent in attempting to achieve acceptable beam profiles to keep polarization moments small at the parity apparatus. Relatively large raw asymmetries obtained from the on-line analysis indicated that the beam convergence was not appropriate to reduce the intrinsic first moment sensitivity to zero.

A delayed start was experienced after the Christmas break due to problems with the cyclotron cooling water system. The beam line 1 combination magnet also failed during this period, severely limiting the ability to shadow the ultrathin (200 μg/cm^2) stripping foil holder with the beam line 1 stripping foil. The remainder of the run was therefore carried out using a much thicker 2.5 mg/cm^2 stripping foil which was freely hanging and therefore did not require the holder to be shadowed inside the machine. Relatively large and variable systematic offsets were found in the raw data, and extra time was spent experimenting with different beam tunes to try to identify the source of the effects.

Analysis of these data is currently under way. The raw data have a statistical error of $\pm 0.4 \times 10^{-7}$ grouped into 14 main data sets according to the beam line helicity tune, but the consistency of the **raw** A_z values on a set-by-set basis is about an order of magnitude worse than this.

Because the December–January data were acquired with a variety of beam tune conditions and two drastically different cyclotron stripping foils, the data sets do not have a consistent net sensitivity to intrinsic first moments of transverse polarization $\langle xP_y \rangle$ and $\langle yP_x \rangle$. For this reason, it is very difficult to take advantage of the technique applied to the re-analysis of the February, 1997 data to reduce the uncertainty in the correction for intrinsic moments using the measured extrinsic moment sensitivities obtained in calibration measurements. Thus far, corrections for intrinsic polarization moments have only been made with the 'tune independent' method using external calibration sensitivities at each PPM. The corrected values are consistent with each other. A reduced χ^2 of 0.8 for 13 degrees of freedom results from this analysis, but unfortunately the correction introduces additional noise in each data set.

The preliminary result for the December–January data from this analysis is:

$$A_z = (0.8 \pm 1.8) \times 10^{-7}$$

where the error bar is dominated by the uncertainty in the correction for intrinsic polarization moments. No residual correlations of the corrected A_z are found with any other helicity correlated beam properties for these data, and the data are consistent with zero systematic offsets associated with the spin direction at the ion source and at the cyclotron stripping foil. It must be emphasized that this result is very preliminary, and the reason for the relatively large error bar is entirely due to the fact that a large enough data set was not obtained with a fixed set of beam and cyclotron tune conditions to utilize the error reduction approach taken with the February, 1997 data. Work is continuing to examine subsets of the data and attempt to apply the latter approach to reduce the systematic error uncertainty.

July–August, 1998 data

The raw results of the most recent July–August, 1998 run are presented in Fig. 3 and Table I. The experimental asymmetries $\varepsilon_\pm$ are defined as: $\varepsilon = \pm(A_z \pm \delta A_z)$ for positive and negative beam line helicity tunes; a total of approximately 250 data hours were acquired, roughly equally shared between states of opposite beam line helicity tune. The beam line helicity tune reversal allows some systematic error contributions such as beam energy modulation to be cancelled by averaging the data. Analysis is now concentrating on extracting the sensitivites to polarization

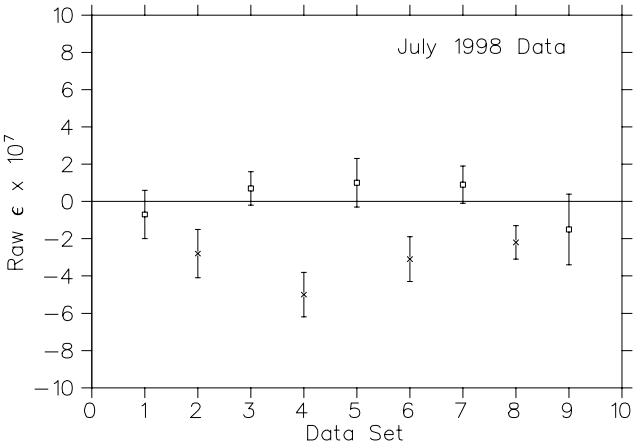

Fig. 3. Raw data from July–August, 1998 parity run. The squares are for positive helicity beam line tunes and the crosses are for negative helicity. The agreement between the data sets is poor compared to Fig. 2 because corrections for first moments of transverse polarization have not yet been applied.

Table I. Raw data summary, July–August, 1998 run. Once sensitivities to $< yP_x >$ and $< xP_y >$ have been determined, the raw asymmetries can be corrected.

Set	Raw ε ($\times 10^7$)	$< yP_x >$ (μm)	$< xP_y >$ (μm)
1 +	-0.7 ± 1.3	10.7 ± 4.1	1.7 ± 2.3
2 −	-2.8 ± 1.3	1.0 ± 1.3	10.0 ± 1.8
3 +	0.7 ± 0.9	14.1 ± 1.7	3.0 ± 1.6
4 −	-5.0 ± 1.2	8.5 ± 2.4	1.9 ± 1.4
5 +	1.0 ± 1.3	9.6 ± 3.2	-2.6 ± 1.8
6 −	-3.1 ± 1.2	3.3 ± 2.2	4.6 ± 1.7
7 +	0.9 ± 1.0	15.2 ± 2.4	0.5 ± 2.0
8 −	-2.2 ± 0.9	7.4 ± 2.6	0.2 ± 1.4
9 +	-1.5 ± 1.9	2.2 ± 4.5	6.8 ± 3.5

moments, and correcting in a way which introduces the least noise.

Summary and outlook

Major progress on data analysis has been made during 1998, resulting in an improved understanding of the sensitivity to intrinsic polarization moments and their effect on the A_z data. It has been shown that the large apparent systematic offset observed in February, 1997 and subsequently in December, 1997 – January 1998 can be understood as a correction due to intrinsic moments of transverse polarization. An analysis technique has been developed to minimize the uncertainty in this correction procedure, but this relies on achieving optimal cyclotron and beam tune conditions over extended periods of time, as experienced in February, 1997. While a data set of comparable size was obtained in December, 1997 – January, 1998, preliminary analysis has thus far been limited to an overall uncertainty that is some 2.5 × larger than in February, 1997 due

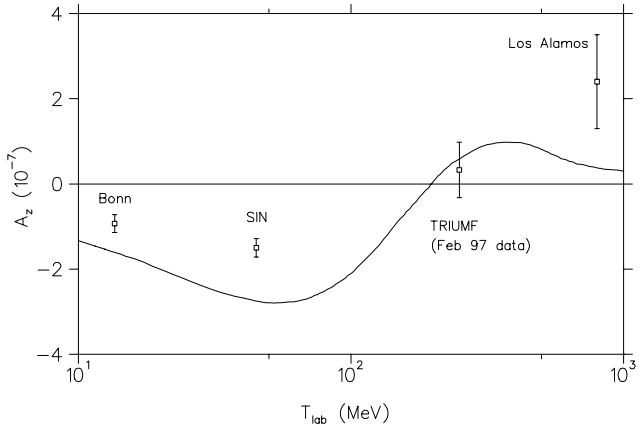

Fig. 4. Theoretical prediction for A_z in pp scattering, calculated by Driscoll and Miller using DDH predictions for the weak meson-nucleon coupling constants, shown with the highest precision existing experimental data. The TRIUMF data point is preliminary, based on the re-analysis of the February, 1997 data set.

to difficulties in assessing the sensitivity to intrinsic polarization moments with sufficient accuracy. Work in progress could substantially reduce the error bar in the most recent data set to the 10^{-7} level, but this remains to be demonstrated. Work is also in progress to re-analyze data taken in 1996 using the new technique.

The result from the re-analysis of the February, 1997 data is shown in Fig. 4 together with a meson exchange model prediction for A_z in the range of $T_{\rm lab} = 10 - 1000$ MeV calculated by Driscoll and Miller [Phys. Rev. **C39**, 1951 (1989)], with weak meson nucleon coupling constants h_ρ^{pp} and h_ω^{pp} taken from the original prediction by Desplanques, Donoghue and Holstein (DDH)[Desplanques *et al., op. cit.*]. Also shown are the highest precision existing experimental data in this energy range. The TRIUMF data point supports the meson exchange prediction at the level of this first result. Preliminary analysis has already indicated that the existing parity data set should be accurate at the $\pm 0.4 \times 10^{-7}$ level (total error bar) or better. An additional 6 week run is planned for summer, 1999, which is expected to complete the experiment. The final result should be available in 2000 and should be of high enough precision to determine uniquely for the first time an experimental constraint on the weak meson nucleon coupling constant h_ρ^{pp}.

Experiment 614
Precision measurement of the Michel spectrum from muon decay
(D.R. Gill, TRIUMF)

As tests of the standard model continue to support its veracity, the need for higher and higher precision measurements increases in importance. Historically one of the best laboratories for testing the electroweak sector of the standard model has been the

decay of the μ. With this in mind a new round of muon decay experiments, with considerable improvement over previous undertakings, is about to get under way at the meson factories, TRIUMF and PSI. At TRIUMF the Expt. 614 collaboration proposes to measure with high precision the differential spectrum, $d^2\Gamma/dXd(cos\theta)$ of positrons from the decay, $\mu^+ \rightarrow e^+\nu_e\overline{\nu}_\mu$ for polarized muons. Here X is the positron energy ($X = 1$ corresponds to the maximum positron energy $E_{\max} = 52.83$ MeV), θ is the angle between the muon spin direction and the positron momentum. The "surface" muon beam with a momentum of 29.8 MeV/c from the M13 beam line at TRIUMF will be used as the muon source.

During 1998 the Expt. 614 collaboration achieved several important milestones. The first of these was the delivery to TRIUMF of all the high precision components of the planar drift chambers (PDC) that the Russian team had undertaken to provide. Following closely were the funding of the U.S. members of the collaboration by DOE and the first substantial project grant for the Canadian team from NSERC. Other milestones include: the completion of the analysis of the 1997 test data on the performance of the prototype PDCs, several Monte Carlo studies and the purchase of the superconducting solenoid required for the experiment.

Full scale prototypes of the Expt. 614 PDCs were constructed and tested in M13 in August, 1997. The analysis of this data was completed in early 1998. The analysis of an event consisted of a search for hits identifiable with a track, an iterative procedure to determine the hit position on the drift circle and the angle of the track relative to the chamber planes, construction of the track and calculation of an average tracking residual. The width of the tracking residuals reflects the intrinsic resolution of the chamber as well as all other factors that may contribute to inaccuracies in the tracking. This includes ingredients such as wire positions and drift distance. In addition, it reflects any biases in the fitting process, as well as the weighting used in the fit. The reasonably narrow width obtained and the level of symmetry of the results provides reasonable confidence in all these factors.

To determine the resolution as a function of position across a wire chamber cell, the widths of the tracking residuals were determined in 10 bins (each 200 μm wide). Employing an iterative procedure, the residuals as a function of drift distance were established. Figure 5 shows the result.

The chamber resolution improves as a function of drift radius due to the increase in ionization statistics. Our result is generally consistent with others (see for example Cindro *et al.* [Nucl. Instrum. Methods **A309**, 411 (1991)]).

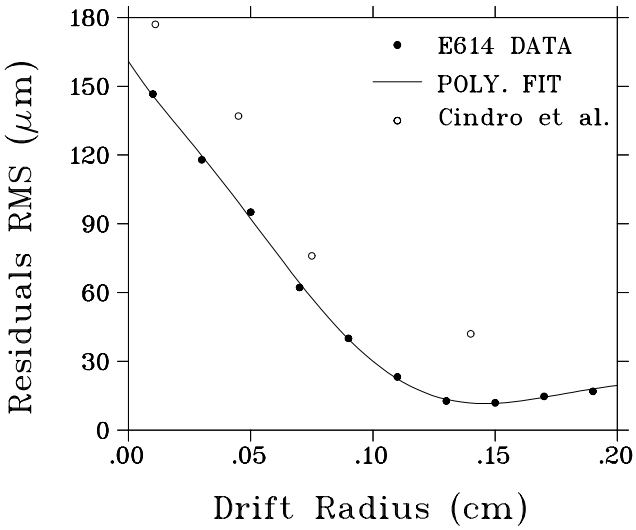

Fig. 5. Chamber resolution as a function of drift radius. The dots are computed from data acquired at 1850 V and a chamber orientation of 0°; the curve is an eight parameter polynomial fit to the data. The circles are data from Cindro *et al.* [*op. cit.*] obtained with a drift chamber that had a cell size of 10.4 mm × 11.4 mm and filled with pure DME gas.

One of the prime purposes of this prototype test was an important decision regarding the final chamber design, whether field wires are required between the sense wires. Installing field wires introduces disadvantages in terms of chamber construction and stability, as well as increasing multiple scattering in the chamber. The no field wire option is, therefore, desired based on this criteria. The lack of field wires, however, results in a weak electric field region away from the sense wires (zero at the midpoint between any two sense wires), and hits may therefore be lost due to poor electron collection from this region. This weak field region raises a concern about the chamber efficiency as a function of distance from the sense wire. To examine this effect the efficiency was calculated as a function of distance from the sense wire for 0° runs resulting in Figure 6. As expected, the lower threshold runs (140 mV) provide the best result, since signals arriving from the weak field region are expected to be small and therefore the most likely to be cut out by a high threshold. This result indicates that the chambers will have a negligible volume of slightly reduced efficiency if constructed without field wires. Construction of the PDCs along the design of those of the prototype tested will therefore begin in early 1999. Another conclusion reached is that the front end electronics of the detector function as expected. Construction of the required complement of these electronics will also begin in early 1999.

The construction of the seven planes and their assembly into the prototype detector for use in this test provided much needed experience in this procedure.

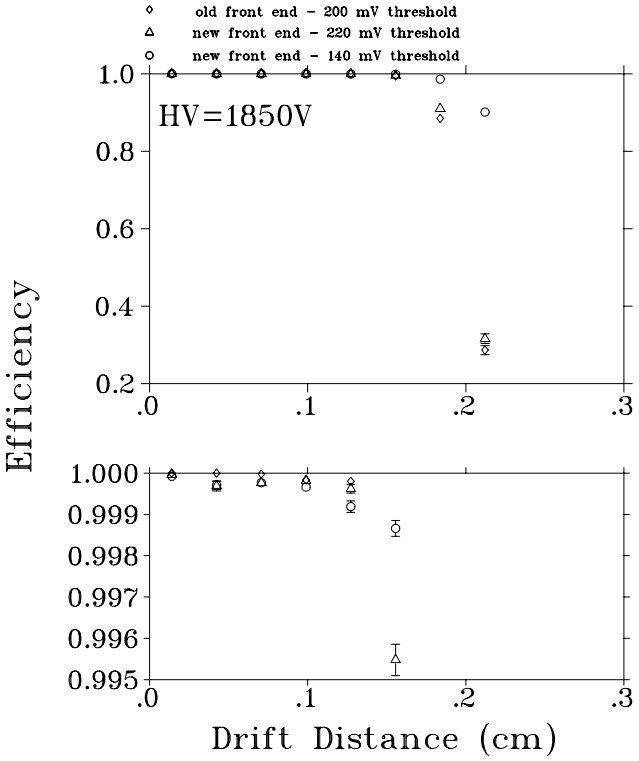

Fig. 6. Chamber cell efficiency as a function of distance from the sense wire for data acquired at 1850 V with a) the old front end at a threshold of 200 mV, b) the new front end at a threshold of 220 mV, and c) the new front end at a threshold of 140 mV. The bottom histogram is an enlarged copy of the top histogram.

As a result several changes were made in the detector design and in the assembly procedure. One of these changes may make it possible to assemble the chambers on a time scale of one year rather than the previously estimated 18 months to two years.

During 1998 several design decisions were made on the basis of Monte Carlo studies of the Expt. 614 detector system. One of those involved the tracking of the incoming muon. A central goal of Expt. 614 is to measure the product $P_\mu \xi$ to a precision of less than three parts in 10^4. The mean depolarization ($< 1 - P_\mu^z >$) must therefore also be less than this in magnitude. The approach used in a previous experiment [Jodidio *et al.*, Phys. Rev. **D34**, 1967 (1986); *ibid.*, **D37**, 237 (1988); Balke *et al.*, Phys. Rev. **D37**, 587 (1988)] at TRIUMF, to measure the muon trajectory before the muon encounters the fringe field (i.e. where the trajectory is linear) was examined via Monte Carlo. To determine if such a measurement would provide the desired information on the stopped muon polarization, two simulated PDCs were placed in the beam line, upstream of the fringe field. The multiple scattering in these detectors modified the relationship between the muon momentum and the muon spin so much that the results could not be used to make a selection. It was therefore decided to study the employment of a very low mass device, such as a time expansion chamber (TEC), in this position. In Monte Carlo simulations, such a chamber was placed upstream of the solenoid fringe field. This chamber, designed to be operated at 20 torr, will be positioned so that the xz and yz measuring sections are just before the entry port in the spectrometer steel, which is ∼160 cm upstream of the stopping target. In the simulation of the TEC the output of the chamber was used to reconstruct the incoming muon track. Correlations between the reconstructed angle with the spin direction of the muon as it stopped in the target were studied. A cut on the polar angle of the initial muon track as measured by the TEC was found which retained ∼12% of all muons stopping in the target while reducing the mean depolarization $< 1 - P_\mu^z >$ of the retained events to $\sim 2 \times 10^{-4}$. This result was obtained using a standard M13 beam with a focus at the fringe field region, 160 cm upstream of the target. For such a tune ∼78% of the M13 flux stops in the target so that the above selection means that only 10% of the incoming muons are finally useful. This success of the TEC concept has led to the decision to complete the design work with the aim of testing a prototype in the summer of 1999. Monte Carlo studies to search for an M13 tune that optimizes the percentage of muons with mean depolarization $< 1 - P_\mu^z > \leq 2 \times 10^{-4}$ will be carried out.

Another design decision, the implementation of pulse height measurements on signals from the proportional chambers (PC) near the muon stopping target was made based on Monte Carlo studies.

μ depolarization in detector materials will occur through the formation of muonium with subsequent spin exchange occurring between the electron and muon. This does not occur in general in pure metals where the lifetime of any muonium that is formed is too short to allow the spin exchange to happen. Obviously the target material will be the highest grade Al possible.

On the other hand muonium can form in many of the materials that make up the detector and may last sufficiently long enough for this spin exchange process to occur. It is necessary to prevent muons stopping in such materials or to be able to "cut" such events during the analysis stage. This issue will be addressed by the use of the proportional chambers adjacent to the stopping target. Nominally the condition that the two upstream PCs see the passing muon while there is no signal from those downstream of the target removes such events. However, this simple scheme may not account for those muons that could lose all their energy and stop in the last upstream PC. The addition of ADCs to the PCs will solve this problem by allow-

ing for a measurement of the energy loss. Monte Carlo simulations were performed to determine the efficacy of this extra information. In the simulation a beam of 29.7 MeV/c μ^+s was tracked until they stopped. As muons entered and exited the PCs, their kinetic energy was recorded and their energy loss in each chamber was entered into a histogram. The mean energy loss per muon in the chambers was ∼0.1 MeV. It was found that, in 10,000 entries, the smallest energy loss recorded by PC(+1) was ∼20 keV. Providing the chamber thresholds can be kept low (≤5 keV), it is therefore unlikely that muons will pass through the target and not be recorded by PC(+1). With the pessimistic assumption that the PC(+1) energy threshold is 25 keV, ∼2 stops in PC(+1) will be missed by a cut at this level per 10^4 stops in the target.

A scatterplot of energy losses in PC(-2) and PC(-1) is shown in the upper-left of Fig. 7 and exhibits two main features: a dense locus of points with a positive slope and a less dense locus with a negative slope. The dense locus with positive slope is due to muons stopping in the target (Fig. 7, bottom left), and the low energy end of this locus is due to those that pass through the target (Fig. 7, bottom right). The less dense locus of negative slope is due to muons stopping in PC(-1). A two dimensional cut along the lower edge of the locus of PC(-1) stops reduced such stops to $2 \cdot 10^{-4}$ of the incident flux while more than 97% of the muons stopping in the target were kept.

The measured P_μ value for muons stopped in $CF_4(ISO)(80:20)$ gas at $B = 2T$ is $P_\mu > 0.985$.

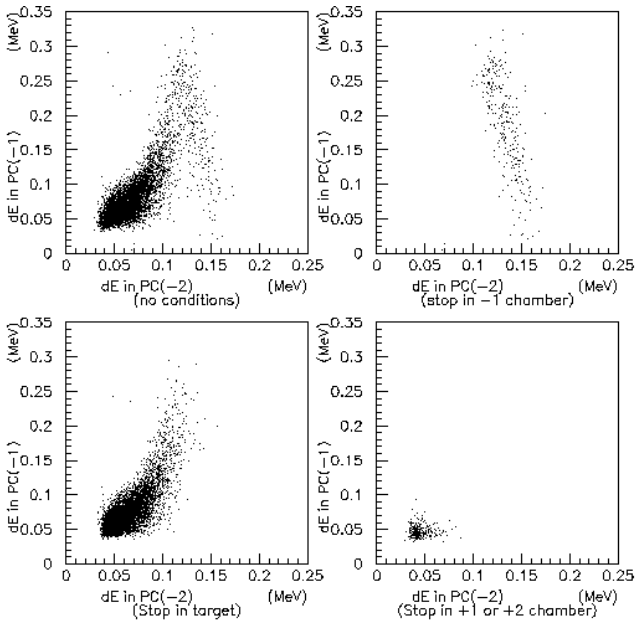

Fig. 7. Energy loss in PC(-1) vs. PC(-2) chambers for various muon stopping conditions. Top left: no conditions; top right: stop in PC(-1); bottom left: stop in target; bottom right: stop in PC(+1) or PC(+2).

According to the above Monte Carlo calculations ≤ $2 \cdot 10^{-4}$ muons stop in PC(-1) and in PC(+1). The shift of $(1 - P_\mu \xi)$ is therefore pessimistically estimated to be $(1 - 0.985) \times 5 \cdot 10^{-4} = 7.5 \cdot 10^{-6}$.

A monitor of the stopping distribution in the target is required. A simple method is merely to count the number of muons passing through the proportional chambers. A Monte Carlo study in which the material determining the range of muons was altered showed that the ratio of the number of muons recorded by PC(+2) to those recorded by PC(-2), $N_{PC(+2)}/N_{PC(-2)}$, and the ratio of PC(+1) to PC(-1), $N_{PC(+1)}/N_{PC(-1)}$, were found to be sensitive to changes in the stopping distribution. These ratios should not be affected significantly by factors such as PC efficiency or muons stopping in PC(-1). For a stopping distribution that was symmetric in the target the ratios $N_{PC(+1)}/N_{PC(-1)}$, and $N_{PC(+2)}/N_{PC(-2)}$ were 0.054 and 0.0173, respectively. Deviations of ±20 μm in degrader thickness produced a significant change in these ratios. It has thus been concluded that the central PCs will provide a reliable monitor of stopping distribution.

The geometry of the original (baseline) detector had equal, 4.8 cm, centre to centre spacings of the PDC pairs (x, y). This geometry presents the possibility that the wavelengths of certain helical tracks would coincide with the period of the chamber pairs, thus producing poor fits in the x or y projection. A Monte Carlo study was therefore made of alternating these spaces such that the distances between the centre of each pair was either 4.8 or 6.8 cm. It was found that this change substantially improved the momentum resolution (see Fig. 8) by increasing the lever arm over which the track position is measured. Little difference was found in the angular resolution for the two cases. The detector will be assembled with spaces between pairs that are not all identical and on average that are larger than the baseline design.

The Expt. 614 solenoid magnet is a used NMR coil, "sister" to a magnet used in an experiment at LAMPF. The LAMPF magnet was not available to Expt. 614. The Expt. 614 magnet was tested at the site of the company from which it was purchased. These tests were observed by TRIUMF personnel sent for that purpose. It was then shipped, at liquid helium temperature, to TRIUMF in September where further tests were performed. The solenoid has no return yoke for the very large field so design work has begun, with construction of this shield scheduled for mid 1999. The field of the shielded magnet will then be mapped in detail.

During 1998 Expt. 614 took possession of a new clean room in the office building. This facility, the old CCD lab modified by TRIUMF to meet the

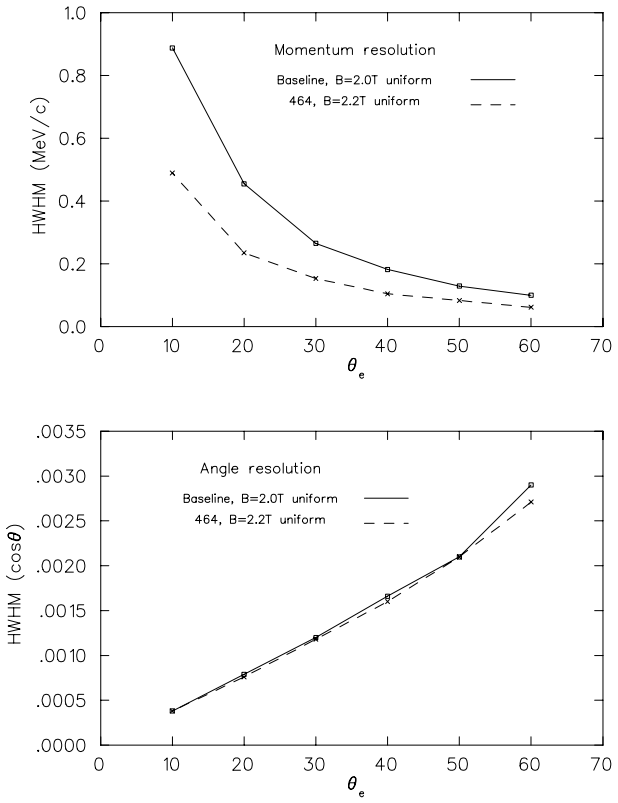

Fig. 8. Top: momentum resolution for baseline spectrometer (solid line), and spectrometer modified to include alternating 4.8 and 6.8 centre to centre spaces (464 option, dashed line). Bottom: angle resolution for same two options.

requirements of Expt. 614, will be used for the assembly of the drift chambers and the proportional chambers. As stated above, this work is to begin in early 1999. The goal of the Expt. 614 collaboration is to assemble these chambers so that it will be possible to be on the floor in late 2000 to begin data accumulation.

Also in 1998 the Expt. 614 collaboration undertook to examine the M11 channel as a potential source of surface muons. The "old wives' tale" was that no surface muons could be found emanating from M11. This undertaking turned out to be non-trivial. The largest changes that were required to make this hunt for polarized muons possible fell to the TRIUMF Power Supply group. Alterations to the power supplies had to be made in order that they would operate at the low currents required for a 30 MeV/c tune. In fact it was found that the septum supply would not operate at the required current so another supply had to be substituted for it. The hunt was a success, M11 is a source of surface muons. The flux is lower than that in M13 but should be useful for tests of Expt. 614 detectors. The μSR people are now considering the possibility of doing some of their work on M11.

In summary, for Expt. 614 1998 was another busy and productive year.

Experiment 705
BNL Experiments 813, 885 and 906
Strange physics at BNL: a search for the *H* particle (BNL 813); a search for ΛΛ hypernuclei (BNL 885) using gas microstrip chambers (705); an experiment to detect ΛΛ hypernuclei via characteristic π-mesonic decays (BNL 906)
(C.A. Davis, TRIUMF)

Experiment BNL 813

In 1998, Manitoba graduate student Liping Gan completed her Ph.D. thesis [Gan, *A study of the sensitivity of the H dibaryon search experiment E813 at BNL through* $(\Sigma^-, p)_{\rm atom} \to \Lambda + n$, Ph.D. thesis (University of Manitoba, 1998)] on the analysis of calibration data for BNL Expt. 813. This experiment searches for the six-quark (uuddss) H particle [Jaffe, Phys. Rev. Lett. **38**, 195 (1977)] by looking for H particle production by means of Ξ^- capture on the deuteron ($\Xi^- + d \to H + n$). Ξ^- particles are stopped in liquid deuterium (see Fig. 9) and the signal of H particle production is monoenergetic neutrons in coincidence with "tagged" Ξ^-s. To interpret our results quantitatively, we have to know both the "tagging efficiency" – that is, the probability that a Ξ^- which we identify as entering the deuterium with the right energy and at the right angle to stop will, in fact, stop – and the neutron detection efficiency. These quantities can be calculated by Monte Carlo simulation, but the work described in Gan's thesis provides an independent check on the Monte Carlo. Instead of Ξ^-s stopping in liquid deuterium, she looked at Σ^- particles stopping in liquid hydrogen, producing a Λ particle and a monoenergetic neutron. The Σ^- particles are tagged in the same

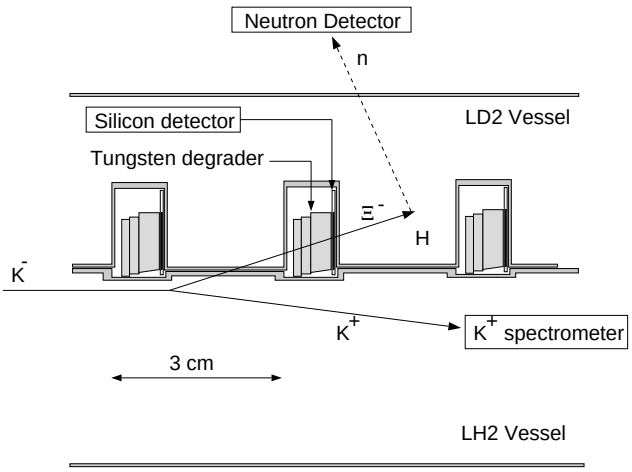

Fig. 9. The BNL E813 version of the H search. Ξ^- particles produced in the liquid hydrogen of the lower chamber of the target are brought to rest in liquid deuterium in the upper chamber. Only three of the twenty target cells are shown.

way as the Ξ^- particles of the main experiment and the monoenergetic neutrons are detected in the same neutron detector. The target and detector geometry is the same and the kinematics of the two reactions are adjusted to be the same. The difference is that the fraction of stopped Σ^- particles which will be captured and form a Λ particle and a neutron is known quite accurately, so the calibration reaction gives us the product of the tagging efficiency and the neutron detection efficiency.

About 10% of the BNL E813 data were taken in 1992. The balance was split between 1993 and 1995. The 1992 and 1993 data have already formed the basis of Ph.D. theses. The 1995 data are now being added to the 1992 and 1993 data and an overall analysis is being done. We expect the final result will be published in 1999.

Details

The H dibaryon is a hypothetical six-quark particle with the same quark content (uuddss) as two Λs. In 1977, Jaffe [*op. cit.*] predicted that the H might be lighter than the $\Lambda\Lambda$ mass of 2231 MeV/c^2, and hence not be able to decay without a change in strangeness – i.e. it would be bound against strong decay. BNL E813 and E836 are experiments designed to look directly for the signature of H formation. As such, these experiments have the advantage that they are insensitive to decay modes and lifetime of the H. BNL E813 looks for H formation through Ξ^- capture on the deuteron and is most sensitive to a lightly bound or slightly unbound H in the mass range from about 15 MeV/c^2 above to 100 MeV/c^2 below the $\Lambda\Lambda$ mass. BNL E836 looks for H formation via the (K^-, K^+) reaction on ^{3}He and is most sensitive to a more tightly bound H in the mass range from about 50 to 380 MeV/c^2 below the $\Lambda\Lambda$ mass.

BNL E836 was completed in 1997 and the result is published in Physical Review Letters [Stotzer *et al.*, Phys. Rev. Lett. **78**, 3646 (1997)]. No evidence for H-production was seen in the mass range from 50 to 380 MeV/c^2 below the $\Lambda\Lambda$ threshold. The upper limit on H-production cross section in this region is approximately an order of magnitude below the theoretical prediction [Aerts and Dover, Phys. Rev. **D28**, 450 (1983)].

BNL E813 uses the two step process, $K^- + p \rightarrow K^+ + \Xi^-$, $\Xi^- + d \rightarrow (\Xi^- d)_{\rm atom} \rightarrow H + n$ (see Fig. 9). The 1.8 GeV/c K^- beam enters the lower, liquid hydrogen, part of the target where the Ξ^- are produced. The outgoing K^+ enter a magnetic spectrometer while the Ξ^- pass through an energy degrader and a silicon detector into the upper, liquid deuterium, part of the target where they stop, forming Ξ^--deuteron atoms. A $(\Xi^-, d)_{\rm atom}$ is predicted [Aerts and Dover, Phys. Rev. **D29**, 433 (1984)] to have a substantial probability of forming an H particle and a neutron. Ξ^-s in the right angular range and having the right energy to stop in the liquid deuterium are tagged. The signature of the production of H particles is the detection of monoenergetic neutrons in coincidence with the tagged Ξ^-s.

In order to interpret the BNL E813 data properly and set a quantitative upper limit on the production cross section, it is necessary to know the product of the tagging efficiency and the neutron detection efficiency. At present, these have been calculated by Monte Carlo simulation. For example, the tagging efficiency was estimated at 0.136 stops per tag [Merrill, Ph.D. thesis (Carnegie Mellon University, 1995)]. The neutron detection efficiency depends on the energy of the neutron and on the pulse height cut. A typical value, for $\beta^{-1} = 3.0$ (57 MeV) and 3 MeV$_{ee}$ threshold, is 38% [Merrill, *op. cit.*], which, when multiplied by the 21% of 4π solid angle of the neutron arrays, gives an overall neutron detection efficiency of 8%.

To check the Monte Carlo calculations experimentally, a (π^-, K^+) calibration run was made. During the 1995 run, data were taken for approximately 7 weeks with a π^- beam and with both the top and bottom chambers of the BNL E813 target filled with liquid hydrogen. The momentum (1.4 GeV/c) of the π^- beam was selected so that the kinematics of the Σ^- particles from $\pi^- + p \rightarrow K^+ + \Sigma^-$ would match that of the Ξ^-s from $K^- + p \rightarrow K^+ + \Xi^-$. The Σ^-s pass through the degraders and silicon detectors between the upper and lower target chambers and stop in the LH_2 of the upper chamber, forming monoenergetic neutrons by means of $\Sigma^- + p \rightarrow \Lambda + n$. This simulates the case in the normal H search configuration, with LD_2 in the upper target chamber, in which the Ξ^-s pass through the degraders and silicon detectors and stop in the LD_2, producing H particles by means of $(\Xi^- d)_{\rm atom} \rightarrow H + n$. Since a stopping Σ^- in the calibration experiment deposits the same energy in the silicon detectors as a stopping Ξ^- in BNL E813, and since it is known that $(45 \pm 3)\%$ [1] of the stopped Σ^-s will give a neutron, analysis of the calibration data will give us the product of the stops per tag and the neutron detection efficiency, allowing us to confirm the Monte Carlo simulation.

The analysis of the calibration data is presented in the Ph.D. thesis of Liping Gan. Figure 10 is taken from her thesis and shows the results of the 1995 (π^-, K^+) run. 1650 events satisfied the tag definition shown. Also shown are two methods of estimating the background under the peak. The polynomial fit is better at low β^{-1} than the background estimated from the untagged neutron spectrum. The monoenergetic neutron peak from

[1] The uncertainty is mainly due to uncertainty in ν, the fraction of stopped Σ^- which will actually form a $(\Sigma^-, p)_{\rm atom}$.

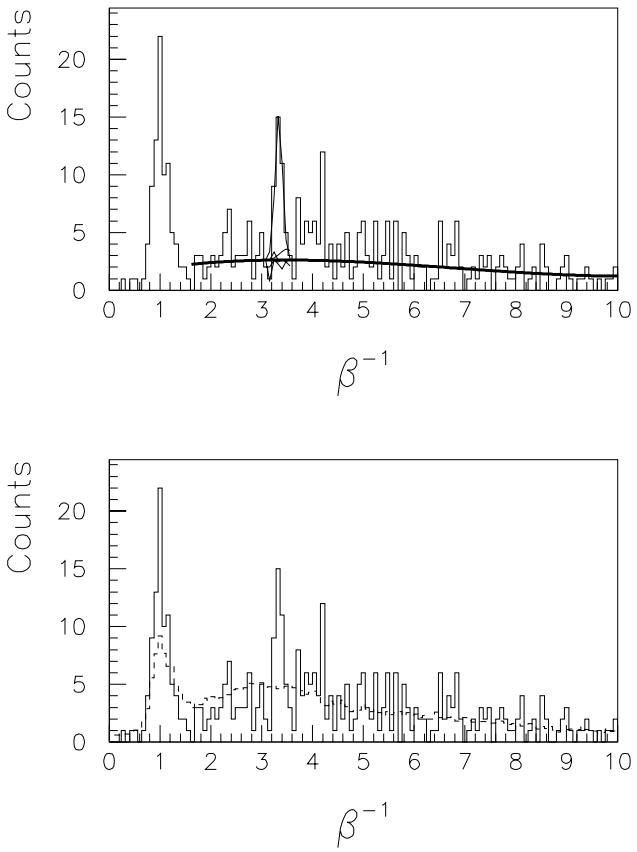

Fig. 10. Neutron β^{-1} spectrum of tagged Σ^- events from the 1995 $\pi^- + p \to K^+ + \Sigma^-$ running. The tag definition is $7.5^\circ \leq \Theta_{K^+} \leq 10^\circ$, and 1.2 MeV $\leq E_{SI} \leq$ 2.2 MeV. The neutron detector threshold is 3 MeV. The background in the top plot was fitted with a third order polynomial, and the background in the bottom plot was fitted with the untagged neutron spectrum.

43.5 MeV neutrons is clearly seen at a β^{-1} of 3.4. The number of neutrons in the peak can be expressed

$$N_{\rm neutron} = N_{\rm tag}\eta_{\rm stop}\nu R_\Lambda \eta_{nd}\,,$$

where $N_{\rm tag} = 1650$ is the number of tagged Σ^- events, $\eta_{\rm stop}$is the number of stops per tag, $\nu = (85 \pm 5)\%$ is the fraction of stopped Σ^- which form a $(\Sigma^-, p)_{\rm atom}$, $R_\Lambda = (53.2 \pm 1)\%$ is the branching ratio for the $(\Sigma^-, p)_{\rm atom} \to \Lambda + n$ reaction [Hepp and Schleich, Z. Phys. **214**, 71 (1968)], and η_{nd} is the product of the neutron detector efficiency and solid angle. The number of neutrons in the peak (in the upper spectrum of Fig. 10) is 28 ± 6, which gives $\eta_{\rm stop}\eta_{nd} = 0.0375 \pm 0.0084$.

Based on this calibration, estimates can be made of the number of neutrons which would be expected from the full BNL E813 data set if H particles are really being formed. By taking the fraction of stopped Ξ^- which will form a $(\Xi^-, d)_{\rm atom}$ from Batty [private communication] and the branching ratio for $(\Xi^-, d)_{\rm atom} \to H + n$ from Aerts and Dover [*op. cit.*], Liping Gan estimates that a peak of about 80 neutrons at 0 MeV H binding or 40 neutrons at 50 MeV H binding would be expected. Such a peak would stand out much more clearly than the calibration peak shown in Fig. 10, and would be easily seen.

All the BNL E813 data from 1992, 1993, and 1995 are now being combined using a consistent set of cuts. At the present time it appears that no statistically significant H production peak will be seen, and that the experiment will set an upper limit. We expect the final result to be published in 1999.

Experiment BNL 885

Experiment BNL 885 is a search for exotic S= −2 systems, namely ΛΛ-hypernuclei, Ξ-hypernuclei, and the H particle, a hypothetical six quark state (uuddss) below the mass of two Λ particles. BNL E885 is a high statistics experiment, necessitated by the lack of data in this sector. For instance, the three candidate events for ΛΛ-hypernuclei [Danysz *et al.*, Phys. Rev. Lett. **11**, 29 (1963); Prowse, Phys. Rev. Lett. **17**, 782 (1963); Aoki *et al.*, Phys. Rev. Lett. **69**, 1729 (1990)] are kinematically incomplete and appear to give inconsistent ΛΛ binding energies. Experiment BNL 885 was carried out in 1996 at the D6 2 GeV K beam line [Pile *et al.*, Nucl. Instrum. Methods **A321**, 48 (1992)] at Brookhaven National Laboratory. The beam line was created for the BNL E813/E836 H particle searches, and is characterized by an excellent K/π ratio ($\sim$ 2–3) and large acceptance (0.065 sr).

During the initial running of BNL E885, kaons incident on a CH_2 target produced Ξ^- hyperons. The Ξ baryons then left the production target, were degraded and stopped in a scintillating fibre array (SciFi), which acted as an active target. The Ξ hyperons are then free to form S = –2 exotic systems with target nuclei. After several weeks of running with CH_2, a target switch was made. The majority of the running time then utilized a chemical vapour-deposited diamond target, in which the Ξ^- is created, stopped, and captured to form ${}^{12}_{\Lambda\Lambda}B$ or other S = –2 objects. A diamond target ($\rho = 3.3$ g/cm^3) was selected given the high density would result in more Ξ^- stops in the target, relative to graphite ($\rho = 2.3$ g/cm^3) or CH_2 ($\rho = 1.1$ g/cm^3).

BNL E885 is sensitive to a variety of channels in the S = –2 sector. Data analysis will search for evidence of the formation and decay of the following doubly strange species:

$(\Xi^-, {}^{12}\mathrm{C})_{\rm atom} \to {}^{12}_{\Lambda\Lambda}\mathrm{B} + n$ (via stopped Ξ^-)
$K^- + {}^{12}\mathrm{C} \to {}^{12}_{\Lambda\Lambda}\mathrm{Be} + K^+$ (direct production)
$K^- + {}^{12}\mathrm{C} \to {}^{12}_{\Xi}\mathrm{Be} + K^+$ (direct production)
$K^- + {}^{12}\mathrm{C} \to H + K^+ + X$ (direct production)
$(\Xi^-, {}^{12}\mathrm{C})_{\rm atom} \to H + {}^{11}\mathrm{B}$ (stopped Ξ^-) .

The AGS delivered beam to the D6 line from March 1, 1996 – June 28, 1996. In this time new apparatus was commissioned, experimental startup problems were ironed out, and production data were gathered. After commissioning and running several weeks with the CH_2 production target, we switched to diamond and received $0.807 \times 10^{12}\, K^-$ on this target, with 7.75×10^8 triggers accepted. The DAQ live time was approximately 75%. Over half of the data were reduced on-line and the cascade production rate was monitored (typically $\sim 600\, \Xi^-/10^9\, K^-$, live-time corrected). Reduction of the data set was necessary to eliminate events in which the secondary particle is a proton misidentified by the hardware triggers as a K^+, for example.

Micro-strip gas chambers

Microstrip gas chambers (MSGC) with an active area of 80×50 mm^2 were instrumented and operated as a vertex detector in the experiment. While MSGC were first introduced a decade ago [Oed, Nucl. Instrum. Methods **A263**, 351 (1988)], they have rarely been used in experiments [Angelini *et al.*, Nucl. Instrum. Methods **A315**, 21 (1992); Geijsberts *et al.*, NIKHEF-H/94-12 (1994); Henkes *et al.*, Proc. Int. Workshop on Micro-Strip Gas Chambers (Lyon, 1995) p.143]. Furthermore, two distinct types of microstrip prints were utilized in these chambers. Prints manufactured with integrated circuit (IC) photolithographic technology have fine tolerances and thin minimum trace widths, but can suffer from a high rate of defects per print and are more costly. Prints constructed with printed circuit (PC) photolithographic technology have coarser tolerances but relatively few defects per print, and are extremely cost-effective. BNL E885 marks the first use, worldwide, of the inexpensive and simple microstrip printed circuit process, "PC-based" MSGC.

In-beam MSGCs are mounted upstream (IM1) and downstream (FM1 and FM2) of the target (see Fig. 11), which consists of an array of chemically vapour-deposited industrial diamond wafers. Drift chambers ID1-3 and FD0-3 provide tracking for beam and scattered particles upstream and downstream of the target; the MSGCs were used to improve knowledge of the interaction vertex. The gas mixture used in the MSGCs at BNL was argon:dimethyl ether (DME) (80:20).

PC x and IC y prints were mounted in the upstream MSGC IM1. Downstream of the target, chambers FM1 and FM2 contained only IC prints (IC x and IC y). Commissioning of the detectors was lengthy due to the difficulties in eliminating oscillations in the on-board microstrip preamplifier, the QPA02, and shielding against rf noise sources.

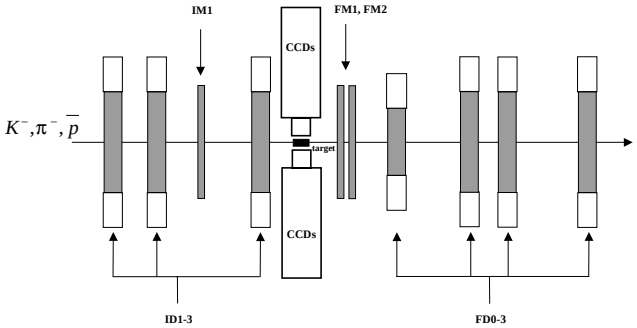

Fig. 11. Position sensitive detectors in BNL E885. For clarity, not all detectors in the target region are shown. MSGCs are IM1 and FM1-2. Drift chambers include ID1-3, FD0-3 (diagram not to scale).

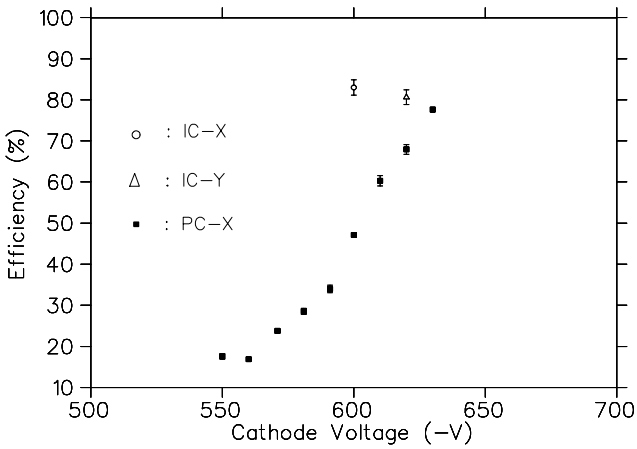

Fig. 12. An efficiency curve for a PC x print in the D6 area at BNL. Higher voltages were not attained due to sparking on the print. Also depicted are operating points for the IC x and y prints.

Figure 12 shows efficiency data for a PC x print, taken during the BNL 885 experiment, with the entire print instrumented. For comparison, the operating point for IC x and y prints is shown. The PC x microstrip will plateau at a higher operating voltage (plateau voltages could not be achieved due to breakdown beyond $V_{x_\mu} = 640$ V), largely due to the thicker metal layer deposited on PC-based microstrip prints, versus that of IC-based prints. The experimental results include known defects due to lithography and high thresholds due to rf noise and are therefore reduced in efficiency. Efficiencies of the MSGCs reached ∼99% in beam tests on sub-sections of microstrip prints, but were reduced in the experiment due to localized lithographic defects on prints, and high discriminator threshold settings.

A paper describing the experience designing, testing and operating the MSGC will be published [Landry *et al.*, Nucl. Instrum. Methods (in press)].

Analysis

BNL E885 analysis is carried out concurrently at Carnegie Mellon University (CMU), Kyoto University, and TRIUMF/University of Manitoba. Analysis efforts at CMU have concentrated on observing the monoenergetic neutron from ${}^{12}_{\Lambda\Lambda}$B formation, as well as analyses of the missing mass spectrum. At Kyoto, ten students have been employed to review the images obtained in the scintillating fibre (SciFi) arrays. Manitoba efforts have concentrated on the MSGC data and the missing mass spectrum.

A missing mass plot for the carbon data set can be used to indicate the production of Ξ^- hypernuclei, expected to be formed in various nuclei [Dover *et al.*, Ann. Phys. **146**, 309 (1983)]. Bound Ξ^- states would be observed as an enhancement in a missing mass spectrum below the quasi-free Ξ^- production peak. Similarly, this spectrum could be cast in terms of binding energy, in which bound states occur below $E = 0$.

A reduced data set of the entire BNL 885 data set has been selected and a time-of-flight alignment performed on a run-by-run basis. A binding energy spectrum can be obtained, making reasonable cuts on kinematic variables such as DCA (distance of closest approach of beam and scattered tracks), Chi-squared of track fits, outgoing kaon mass, etc. Figure 13 shows a preliminary binding energy spectrum, produced including kinematic variable cuts, for the reduced carbon data set. The binding energy is defined as the missing mass minus the sum of the ^{11}B and Ξ^- masses, or missing mass – 11.5738 GeV/c^2. No clear indication of a peak in the bound region is seen. However, there are a significant number of counts in the bound region which have to be accounted for, and cleaned up through further calibration and energy-loss corrections.

Final analyses in the form of Ph.D. theses and publications are expected in 1999.

Experiment BNL 906

The D6 line at the Alternating Gradient Synchrotron at Brookhaven National Laboratory, the most intense and pure source of $\sim 2\frac{\mathrm{GeV}}{c}$ kaons available, was again used this year to explore the double strangeness frontier. The (K^-, K^+) reaction is used to transfer two units of strangeness (S = –2) to a nuclear or two-baryon system.

Another search for doubly strange hypernuclei using a cylindrical drift chamber and a beryllium target (BNL E906) was run on the D6 line in September–November. BNL E906 also serves as an H search and as a search for hyperfragments. Though several weeks of data were taken, additional data will be required in the near future as less than half of the proposed data set was realized.

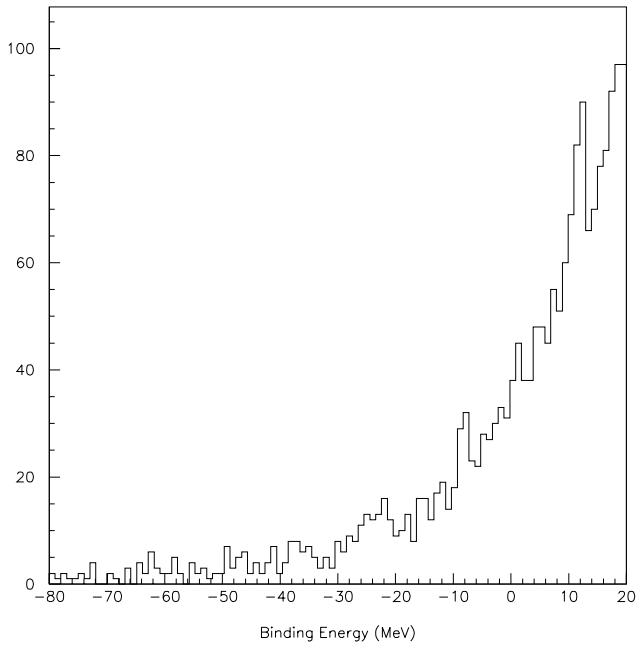

Fig. 13. Preliminary binding energy spectrum for carbon data set.

The ATLAS experiment at the LHC

(C. Oram, TRIUMF)

As described in detail in the 1996 Annual Report, ATLAS is building a general purpose *pp* detector which is designed to exploit the full discovery potential of the Large Hadron Collider (LHC) at CERN. The TRIUMF group is responsible for the engineering of the hadronic endcap (HEC) calorimeter, and the feedthroughs for the endcap cryostat. For the HEC, this year has seen the end of prototype and pre-production construction and the beginning of module production, while for the feedthrough project, at the University of Victoria, the project is completing the prototype stage. The simulation of the HEC, previously done using GEANT 3, is being re-written in the GEANT 4 framework by a collaboration between ATLAS and the GEANT 4 group headed by TRIUMF personnel.

Physics goals

The present theoretical understanding of elementary particles is in the context of the standard model. The standard model is a remarkably successful model, providing predictions which have been consistently confirmed by experiment for over two decades. Its agreement with experimental results, to enormous accuracy in some cases, makes it the most accurately verified model in science. Of the many elementary particles contained in the standard model, only the Higgs remains to be discovered. The central goal of ATLAS is the search for the Higgs particle.

There are good theoretical reasons to believe that the discovery of the Higgs will at least contain hints at, and more likely direct evidence of, what lies beyond the standard model. If the Higgs is composite, its existence requires as yet unknown ultra-strong forces. If it is elementary, it would be the only spinless particle to be discovered so far. There is a theoretical 'naturalness' problem for the masses of spinless particles. In the standard model, which is a highly nonlinear dynamical system, the elementary particles tend to take on the heaviest of all possible mass scales which in such a model are at inaccessible energies and inconsistent with other requirements of the model. All other particles discovered thus far have natural mechanisms, such as gauge and chiral symmetries, for protecting their masses so that they can lie in the observable range. For the Higgs particle, there is no such symmetry in the present model. The only theoretical scenarios which leave the Higgs particle light enough to observe are hypothetical ones, either technicolour or supersymmetry, both radical departures from the present structure of the standard model. If Higgs is seen at LHC, one of these scenarios should be seen at the same time.

Particle theory has progressed enormously over the last few decades with many appealing scenarios for physics beyond the standard model. The most likely of these is supersymmetry and the boldest of these is superstring theory. These theories are intimately related and are both radical ideas which promise a new conceptual framework for understanding elementary particles. Though far from being complete theories so far, there are superstring models which resemble the standard model in their low energy limit. These models have a great appeal as they contain a unification of fundamental forces which includes gravity. They have already had substantial impact on gravitational physics where, for example, in addition to the long sought reconciliation of gravity with quantum mechanics, they have been used to derive a fundamental understanding of black hole thermodynamics. Superstring theory is still in its infancy, but progress has been dramatic and the promise of great things to come has captured the imagination of a substantial fraction of the world's theoretical particle physicists.

The present theoretical view is that the conventional grand unification of the strong, weak and electromagnetic forces can only work in the supersymmetric extension of the standard model. In that model, the grand unified energy scale is only two decades below the Planck scale, the ultimate energy where spacetime itself has quantum fluctuations. It is not out of the realm of imagination that, at energy scales where supersymmetry would be observed, evidence for an ultimate theory of everything, at least everything that can exist once spacetime is formed, is within human grasp.

Experiments at LHC, where the ATLAS detector will take data, will probe the energy region where the Higgs particle, possibly supersymmetry, or other structures will be visible. This will be the first experimental probe of an energy region where fundamentally new physics is expected to occur in many years. There is every reason to believe that the results will be among the most dramatic ever.

Basic ATLAS design considerations

The most prominent issue for the LHC is the quest for the origin of the spontaneous symmetry-breaking mechanism in the electroweak sector of the standard model (SM). This is related to one of the most fundamental questions of physics: What is the origin of the different particle masses? New direct experimental insight is required to answer this question.

One of the possible manifestations of the spontaneous symmetry-breaking mechanism could be the existence of a SM Higgs boson (H), or of a family of Higgs particles ($H^{\pm}$, h, H and A) when considering the minimal supersymmetric extension of the standard model (MSSM). The Higgs search is therefore used as a first benchmark for the detector optimization. For the SM Higgs, the detector has to be sensitive to the following processes ($\ell = e$ or μ) in order to cover the full mass range above the expected discovery limit of LEP of about $m_H > 90$ GeV:

$H \to b\bar{b}$ from WH, ZH and $t\bar{t}H$ using a $\ell^{\pm}$ and b-tagging,
mass range $80 < m_H < 100$ GeV;

$H \to \gamma\gamma$ mass range $90 < m_H < 150$ GeV;

$H \to ZZ^* \to 4\ell^{\pm}$
mass range 130 GeV $< m_H < 2m_Z$;

$H \to ZZ \to 4\ell^{\pm}, 2l^{\pm} + 2\nu$
mass range $m_H > 2m_Z$;

$H \to WW, ZZ \to l^{\pm}\nu + 2$ jets, $2\ell^{\pm} + 2$ jets
from WW, ZZ fusion using tagging of forward jets for m_H up to about 1 TeV.

The sensitivity of ATLAS to the standard model Higgs is displayed in Fig. 14.

In addition to signatures similar to these, the MSSM Higgs searches also require sensitivity to processes such as:

$A \to \tau^+\tau^-$ $\to e\mu + \nu$'s
$\to \ell^{\pm}$ + hadrons + ν's;

$H^{\pm}$ $\to \tau^{\pm}\nu$ from $t\bar{t}$ $\to H^{\pm}W^{\mp}b\bar{b}$ and using $\ell^{\pm}$ tag and b-tagging.
$\to$ 2jets

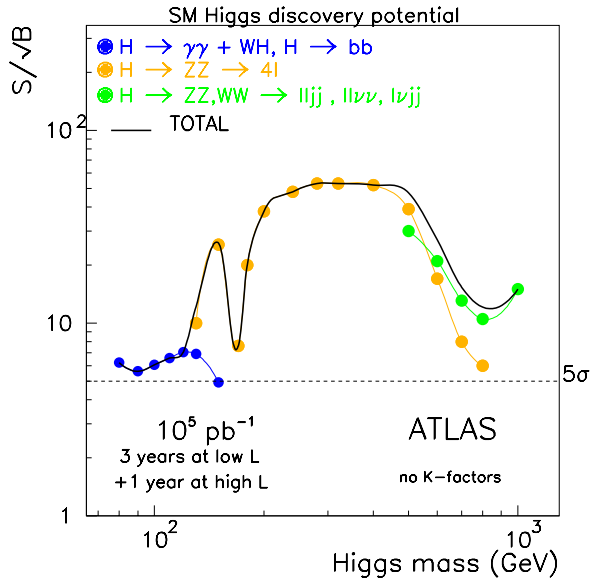

Fig. 14. Expected significance in ATLAS of standard model Higgs boson signal, as a function of Higgs mass, for integrated luminosity of $10^5 \mathrm{pb}^{-1}$ for several decay channels.

The observable cross sections for most of these processes are small over a large part of the mass range to be explored at the LHC. Hence it is important to operate at high luminosity, and to maximize the detectable rates above backgrounds by high-resolution measurements of electrons, photons, and muons.

Canada's participation in ATLAS

The Canadian group consists of 35 grant eligible physicists from TRIUMF, University of Alberta, Carleton University, CRPP, UBC, University of Toronto, University of Victoria, and York University. We are strongly involved in three construction projects centred around detecting hadrons in the endcap region: the hadronic endcap project, the hadronic portion of the forward calorimeter project, and the pipeline electronics for calorimetry. In addition we are committed as part of our common project contribution to providing the feedthroughs for the two endcap cryostats. TRIUMF is directly involved in all these projects and in the physics simulations.

The hadronic endcap project

The hadronic endcap calorimeter (HEC) is a liquid argon sampling calorimeter with copper absorbers [ATLAS Collab., ATLAS Liquid Argon Technical Design Report (1996)]. A concise overview of this design was provided in the TRIUMF 1996 Annual Report.

Hadronic endcap module production

This year saw the major milestone of successfully passing the Production Readiness Review process at CERN. This process reviews the design and quality control aspects of the design, its aim is to provide ATLAS with a confidence that the sub-detectors will all be of high quality and reliability. Successful completion authorizes the series production to proceed at the HEC sites. The successful completion by the HEC group allowed production to start this fall at all the HEC sites (in Germany, Russia, and Canada). Mechanical aspects of the construction project are overseen by the TRIUMF group. To pass this review the design had to be finalized. While only minor engineering changes had to be made from the pre-production module, the choice had to be made of the technical realization of the high resistive coating. A review committee from Mainz and MPI (Munich) was struck, and the decision was made to use carbon loaded kapton rather than a carbon loaded paint technique. The carbon loaded kapton technique was originally proposed by the detector group at TRIUMF.

Starting in November, the clean room in the MESA was fully in use manufacturing the production readout boards for the HEC. The brake press in the TRIUMF Machine Shop has been heavily used, cutting out components of the detector. Using the brake press and an adaptation of a technology called a steel rule die, commonly used to cut out boxes and shoe leathers, we stamp out nearly all the materials that go in the liquid argon gaps of the HEC. These materials are then either shipped to module stacking sites (including TRIUMF), to Russia for assembly into EST boards, or stay at TRIUMF for assembly into readout boards.

Also in November, copper plate production started at the University of Alberta, for absorber plates for modules to be stacked at TRIUMF. This production is undertaken on a milling machine purchased using a loan from TRIUMF. First plate delivery to TRIUMF will be in early 1999, when module stacking will start in the meson hall clean room. Final manufacture of tooling for this clean room area was proceeding through the fall. Module stacking should start in early 1999.

Test beam measurements of hadronic endcap modules

Two test beam periods on the CERN H6 beam line this year have tested the performance of the pre-production modules of the calorimeter. The H6 beam line provides beams from 20 to 180 GeV. The April test beam data has been analyzed, while analysis of the second period is on-going.

The layout of the beam defining collimators, beam position measuring MWPCs, the collimator and liquid argon cryostat is shown in Fig. 15. In the cryostat are 4 modules of the HEC. Because of limited space they are orientated with their plates perpendicular to the test beam, rather than pointing in a psuedo-rapidity geometry as they will be in ATLAS. This causes the beam to impinge on significantly more readout channels than will be the case in ATLAS, thus increasing

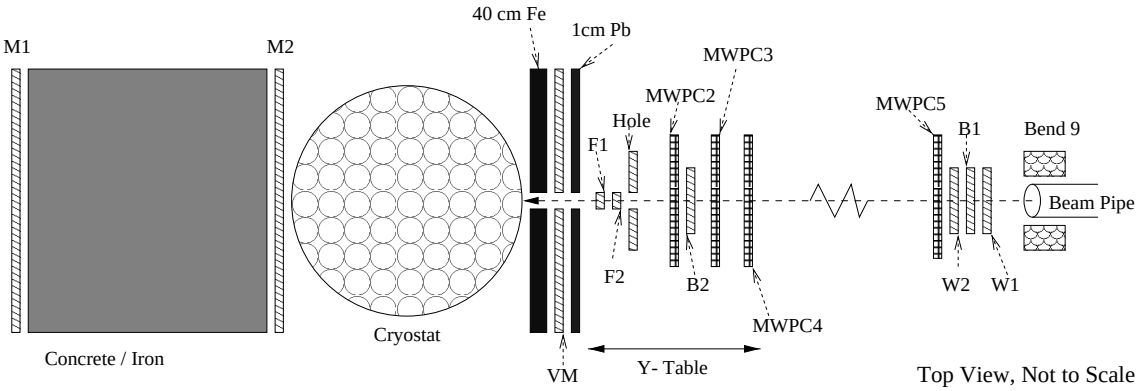

Fig. 15. Set-up of the HEC test beam area at the CERN SPS H6 beam line.

the observed electronic noise to the energy resolution. The impact points of the centre of the beam on the front face of the calorimeter are shown in Fig. 16, along with the tranverse readout segmentation on the front face. The longitudinal (or depth) segmentation of the calorimeter is in three depths, the first 20 cm, the next 40 cm, and finally the last 80 cm of copper.

The pulse height from each readout segment is collected in 25 ns time slices. In a typical event there are about 6 adjacent time slices significantly above the noise. Digital filtering [Cleland and Stern, Nucl. Intrum. Methods **A338**, 467 (1994)] is used to optimize the signal-to-noise ratio. Results of this analysis, as analyzed by the University of Victoria group [Dobbs *et al.*, ATL-COM-LARG-98-009], are shown in Figs. 17 and 18 for electrons and pions respectively. Comparison of these results with Monte Carlo simulations shows the calorimeter is performing as expected, and meets ATLAS design requirements.

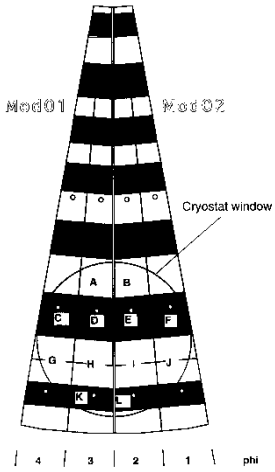

Fig. 16. The geometric layout of the four beam impact positions (D, E, H, and I) on the front face of the HEC calorimeter modules.

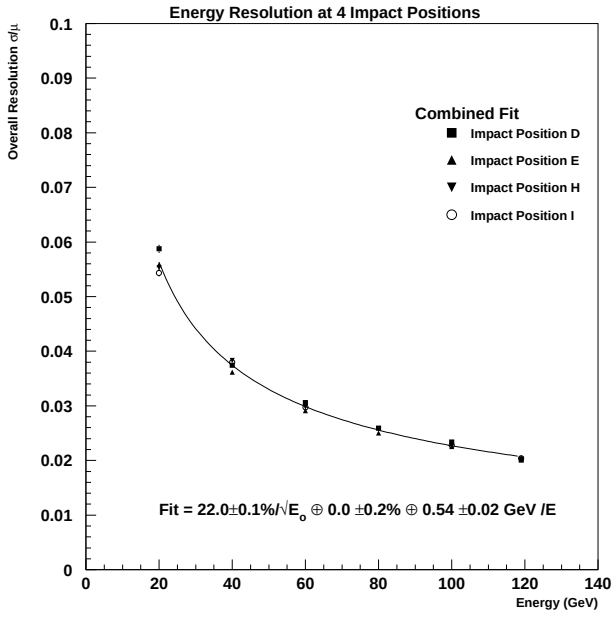

Fig. 17. Measured electron energy resolution: 20–120 GeV.

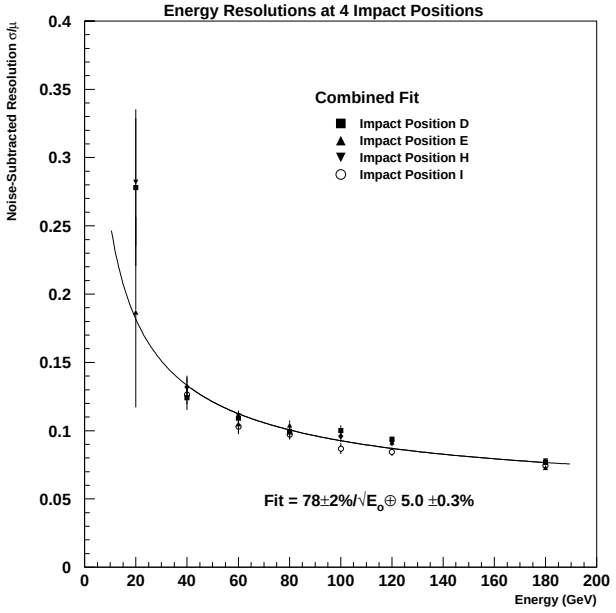

Fig. 18. Pion energy resolution from 20 to 180 GeV, fit over the four beam impact positions.

Study of rare K decays
BNL 787
(D. Bryman, TRIUMF/Victoria)

The rare kaon decays $K^+ \to \pi^+ \nu\bar{\nu}$ and $K_L \to \pi^0 \nu\bar{\nu}$ offer unique opportunities to scrutinize phenomena associated with quark mixing and the origin of charge-parity (CP) non-invariance.

BNL 787 has presented evidence for the decay $K^+ \to \pi^+ \nu\bar{\nu}$ [Adler *et al.*, Phys. Rev. Lett. **79**, 2204 (1997)] based on the observation of a single clean event from data collected in the 1995 run of the AGS. The branching ratio indicated by this observation ($4.2^{+9.7}_{-3.5} \times 10^{-10}$) is consistent with the standard model expectation although the central experimental value exceeds it by a factor of four.

The expected sensitivity from data currently under analysis (taken in 1995–97) is ∼2.5 times that of the 1995 data alone. Subsequent to the initial publication, improvements in the analysis have resulted in background rejection that is ∼3 times greater (a background level of 1×10^{-11}), with no loss in acceptance and results of the analysis of the larger data set are expected shortly. BNL 787 is expected to reach an ultimate single event sensitivity below 10^{-10} by the end of the 1998 running period.

The results presented so far relate only to the relatively clean phase space region above the $K^+ \to \pi^+\pi^0$ ($K_{\pi 2}$) peak. Progress is also being made to access the region below the $K_{\pi 2}$ peak in order to roughly double the sensitivity, but here the background rejection is much more difficult. Using 1989 data, the published upper limit for this was 1.7×10^{-8} (90% C.L.) [Atiya *et al.*, Phys. Rev. **D48**, R1 (1993)] based on no candidate events. The most serious background comes from the decay $K_{\pi 2}$, where the π^+ loses its energy in the target by a nuclear scattering while the detector fails to detect either of the two photons from the π^0 decay. In addition to substantial upgrading of the photon veto system, π/μ identification has since been improved by three orders of magnitude due to the better momentum resolution and demultiplexed range stack scintillators. At present, the analysis of 1995–97 data is in progress in parallel with the analysis of the region above the $K_{\pi 2}$ peak. The expected sensitivity from the 1995–97 data is at the level of the SM prediction with S/N≈ 1.

In 1998 the first published limit on the decay $K^+ \to e^+\nu\mu^+\mu^-$ was obtained by the BNL 787 collaboration [Adler *et al.* Phys. Rev. **D58**, 012003 (1998)]. The result $B < 5.0 \times 10^{-7}$ is consistent with predictions from chiral perturbation theory. This decay mode is a particularly good test of the chiral expansion because the structure dependent terms dominate over the inner bremsstrahlung term due to helicity suppression.

BNL 949 – $K^+ \to \pi^+ \nu\bar{\nu}$

If the branching ratio is as high as the central value of the current result (although there is a large statistical uncertainty), new physics would be indicated. To fully explore this possibility or to make a precise measurement of the $t - d$ quark coupling $|V_{td}|$ (assuming the SM value for the branching ratio), a new measurement has been proposed. BNL 949 has been designed to obtain a single event sensitivity of $(8\text{–}14) \times 10^{-12}$ by means of modest upgrades of the present BNL 787 detector.

The detection of $K^+ \to \pi^+ \nu\bar{\nu}$ (a single incident K^+ followed by the decay to a single π^+ of momentum $P < 227$ MeV/c and no other observable products) requires suppression of all backgrounds to well below the sensitivity for the signal. The two most significant backgrounds are the two-body decays $K_{\mu 2}$ and $K_{\pi 2}$. The other significant background comes from either a π^+ in the beam scattering into the detector or from K^+ charge exchange (CEX).

The primary requirement for the improved experiment BNL 949 is to stop more K^+ mesons near the centre of the detector without increasing the instantaneous rates in the detector. This requires more proton flux from the AGS, but by using an increased duty factor and a lower kaon momentum, the instantaneous beam rate is essentially unchanged. At lower kaon momentum the efficiency for stopping kaons in the target increases while the instantaneous rates due to other sources decrease. Additional improvement arises from longer running time and from increased trigger and DAQ efficiencies. Modest upgrades to the BNL 787 detector and DAQ are needed, primarily to reduce backgrounds in the region below the $K_{\pi 2}$ peak and to satisfy the increased DAQ bandwidth requirements corresponding to the increased sensitivity.

Additional photon veto detectors will be installed, principally a 'barrel veto liner' (BVL), between the range stack and present barrel photon veto, and new photon detectors along the beam axis. The BVL system consists of 48 modules of Pb scintillator arranged in 48 azimuthal sectors. This system is complete and installation will commence after BNL 787 completes data-taking at the end of 1998. The BVL adds critical live material in a thin region of the detector near 45°, and thus is expected to improve the photon vetoing power of the entire detector. It will be especially effective in reducing the $K_{\pi 2}$ background in the region below the peak.

The BNL 787 photon veto thickness is ≤ 7 radiation lengths (X_0) along the beam line in the forward and backward directions. For photons at the low end of our energy range this implies a pass-through inefficiency as high as a few percent. It is important to

reduce this inefficiency in order to suppress the $K_{\pi 2}$ background below the peak. This can be partly accomplished by adding a small supplemental veto counter downstream of the scintillating fibre stopping target. In the upstream direction, three strategies will be used to improve the photon veto efficiency:(i) add several radiation lengths to the existing lead glass detector and increase the radius, (ii) replace the lucite hodoscope light guides by wavelength shifting (WLS) fibres (this allows the installation of active photon veto elements. Another improvement will be the use of triangular-shaped hodoscope elements which will result in better hodoscope position resolution by up to a factor of 5.); and, (iii) modify the beam instrumentation support structure to allow the addition of an annular calorimeter of up to 10 radiation lengths of pure CsI or CeF_3.

The DAQ is FASTBUS based, with front-end readout into SLAC scanner processors (SSP). The data are transferred via the FASTBUS cable segment to VME processors (200 MHz Power PCs). The data are transferred between spills from the VME processors to a 4-CPU SGI Origin 200. The data transfer capability was demonstrated to be >50 Mbytes per spill. The system as currently configured can maintain 80 Mbytes/spill. The dead time was ∼17% per MHz of stopped kaons (KB) (down from 28% in 1995). The DAQ system has been substantially upgraded already. The addition of a fourth cable segment and VME processor are needed for 10^{14} protons/pulse running. Other modest trigger and DAQ efficiency improvements should provide an additional 15% gain. We can also make improvements of ∼10% in the efficiency of our off-line production software. Other more extensive improvements to the trigger/DAQ system using extended programmable logic devices (ELPD) to implement a level 0 pattern finder and a pipelined trigger transmitter are presently under study and may yield up to a factor of 2 gain in sensitivity.

The net increase in sensitivity per year for BNL 949 (relative to the published 1995 result) is expected to be a factor of ∼13.

BNL 926 – $K_L \to \pi^0 \nu\bar{\nu}$

During 1998, some effort began aimed at prototype detector development for a new experiment designed to detect and study $K_L \to \pi^0 \nu\bar{\nu}$ for the first time. The goal of AGS experiment 926 is to observe and definitively measure the rate of this decay. We aim to unambiguously detect a large sample of events so that η, the SM CP violation parameter, can be determined to better than 15% accuracy without serious interference from background or systematic effects. We have scoped the experiment for a sensitivity of approximately 6×10^{-13} allowing for nearly an order of magnitude contingency to meet the goal of a successful measurement if the branching ratio is at least 10^{-11} as predicted by the SM.

In order to make a measurement at the level expected in the SM, the most important means of eliminating unwanted events will be to determine that nothing other than one π^0 was emitted in the decay, i.e. to veto any extra particles. The most difficult mode to suppress is $K_L^0 \to 2\pi^0$. Good photon veto detection efficiency comparable to what has been achieved in BNL 787 will be required. However, to increase the probability that the source of the observed signal is truly the $\pi^0 \nu\bar{\nu}$ mode, additional information is needed. The K_L^0 momentum will be measured using time-of-flight by employing very low momentum kaons produced by a highly time-structured proton beam. Finally, angular and energy measurements for each photon from π^0 decay will be obtained from a preradiator/calorimeter. Such a system imposes kinematic constraints allowing event-by-event reconstruction in the K_L^0 centre of mass frame making a large fraction of the phase space available for detection.

A GEANT Monte Carlo study of the proposed BNL 926 detector has been done at TRIUMF. The simulation included the effects of the varying position of the K_L decay vertex, solid angle acceptance (including the beam hole), and reconstruction efficiency in the photon preradiator. The existing simulation includes photon conversion and reconstruction, phase space acceptance and cuts designed to suppress the major backgrounds (e.g. missing energy, missing mass and photon energy sharing). Preradiator angular resolution from the detector simulation is approximately 25 mrad. The inefficiency due to accidental spoiling of good events is estimated to be < 10% for a threshold of a few MeV and a timing window of 2 ns. The expected number of events to be accumulated is about 50. The single event sensitivity of the experiment would be approximately 6×10^{-13} if not limited by background.

At TRIUMF we are designing and constructing preradiator prototypes. The requirements of the preradiator include a photon angular resolution of approximately 0.02 r, a photon conversion efficiency of about 0.7 (1.5 X_0), a good measurement of the deposited energy and as short as possible linear extent. The principle we will employ is to measure the x and y positions and directions of the first electrons in the shower in a series of thin converter/detector modules. To keep multiple scattering of these electrons at the 0.02 r level each detector module will be ≤0.05 X_0. Since our position resolution will be roughly 200 μm, the detector modules must then be separated by about 1 cm.

The full preradiator will employ 42 layers. Each layer consists of a 2 mm thick × 16 cm wide scintillator (either scintillator plate or arrays of fibres), a layer

of drift chambers or straw tubes with sense wires separated by 10 mm and 5 mm wide cathode strips running perpendicular to the wires, and a 0.035 X_0 thick metal radiator. Mechanical rigidity may be given to a module by pleating the metallic radiator, thus avoiding the need for heavy frame structures around the beam region. The thicknesses of scintillators and radiators are similar to that of the calorimeter so that the energy resolution will be largely unaffected by the preradiator.

To confirm the expectations for the preradiator performance a 10-layer preradiator prototype module is under development. The prototype detectors will be tested at TRIUMF and at the National Synchrotron Light Source (NSLS) at BNL in conjunction with calorimeter prototypes.

Hypernuclear spectroscopy at DAΦNE
FINUDA
(T. Bressani, Torino)

TRIUMF has been involved in the FINUDA experiment at DAΦNE for several years. Our contributions have included construction at TRIUMF of the 20 low-mass drift chambers, and tests using TRIUMF beams of the prototype neutron counters, silicon microstrips, and straw tubes. An extension of the experiment to study the reaction $K_L n \to K^+ p$ has been accepted by the DAΦNE Scientific Committee.

The experiment has been delayed due to the delayed startup of DAΦNE and due to problems with the FINUDA solenoid magnet.

DAΦNE status

In 1998 the accelerator has been commissioned in the "Day One" configuration, i.e. without solenoid magnets in the interaction regions. First collisions were observed in March with the collider in single bunch mode; a luminosity of 2×10^{28} was achieved. Following replacement of a defective dipole magnet, single bunch luminosities exceeding 10^{30} were achieved in October. In November multibunch collisions were observed with a luminosity of 10^{31}. The initial experiments are presently being installed in the collision regions.

FINUDA status

The FINUDA solenoid field was extensively mapped and finally declared acceptable. It has been delivered to Frascati and will be installed in early 1999. Installation of the detector elements is scheduled for summer, 1999. The full detector system, sans magnet, is being commissioned using cosmic rays.

TRIUMF/Univ. Victoria contributions

The outermost tracking layer is an array of 2424 aluminized mylar straw tubes arranged in three superlayers (one axial and two approximately $\pm 13^\circ$), each superlayer with two sub-layers of staggered straws. The inner radius is 110 cm with a full length of about 255 cm for axial superlayers. The basic array element is a 0.03 mm-thick mylar straw, with a 15 mm inner diameter, for a total of 2424 straws. In this year, we have assisted with the installation and commissioning of the straw tube chambers in the clepsydra, which will be subsequently mounted in the solenoid.

The initial experimental program for FINUDA has stressed high resolution hypernuclear spectroscopy. However, there is also the possibility to study the hadronic weak interaction through the observation of the $\Lambda N \to NN$ and $\Lambda NN \to NNN$ interactions. This allows us to address the parity-conserving amplitudes as well as the parity-violating amplitudes studied by Expt. 497 at TRIUMF. The present data have large errors and do not agree well with theory.

At TRIUMF we have incorporated into the FINUDA simulation an event generator for weak decays based on a code obtained from A. Ramos. Briefly, the probabilities for $\Lambda N \to NN$ and $\Lambda NN \to NNN$ reactions are calculated using the one-pion-exchange mechanism, and then the propagation of these nucleons through the nucleus are considered. This results in the generation of nucleons fully correlated in energy and angle which can be tracked through the detector. The very thin targets used in FINUDA allow us to observe efficiently the low energy nucleons which are most sensitive to the different model predictions.

FINUDA collaborators (Canada only) are: Art Olin, George Beer, and Pierre Amaudruz.

Spin structure of the nucleon
HERMES
C.A. Miller, TRIUMF; M.C. Vetterli, TRIUMF/SFU; M.G. Vincter, Alberta)

Deep inelastic lepton-nucleon scattering (DIS) experiments have been crucial in the development of our current understanding of the quark-gluon structure of nucleons. In the last decade, intense interest has focused on how the spins of the quarks and gluons contribute to the spin of the nucleon. Information about this spin structure can be obtained from the cross section asymmetry measured in deep inelastic scattering of longitudinally polarized leptons from polarized nucleons with their spins parallel or anti-parallel. A series of such inclusive DIS experiments at CERN, SLAC and DESY on both proton and 'neutron' targets, recently culminating in remarkable precision, present a coherent picture. Early indications of the relatively small net contribution of the quark spins to the nucleon spin have been confirmed. Newly published data from HERMES, together with new data from SLAC at 50 GeV,

are adding to the inclusive data set as a function of Q^2, thereby improving global fits of polarized quark distribution functions. However, it is now realized that inclusive measurements are intrinsically limited in what more they can offer.

Semi-inclusive measurements involving the detection of a leading hadron in coincidence with the scattered lepton offer a means of 'flavour-tagging' the struck quark to help isolate the contributions to the nucleon spin of the individual quark flavours, including the sea quarks. This is a central theme of the HERMES experiment, which is unique among polarized DIS experiments in two important respects. The targets are atomically pure nuclear-polarized H, D or ^{3}He gas in a high energy polarized electron storage ring. Hence the targets are undiluted by unpolarized nucleons in 'extraneous' materials. Also, the spectrometer detecting the scattered lepton, often in coincidence with hadron(s), combines substantial acceptance with hadron identification capability. Pion identification was included from the beginning, and kaon identification has been added for 1998. A schematic diagram of the experiment is shown in Fig. 19 and a detailed description can be found in [HERMES collaboration, Nucl. Instrum. Methods **A417**, 230 (1998), hep-ex/9806008].

While data on semi-inclusive hadron production have been produced by SMC, their statistical precision is limited and SMC does not identify the hadron type. HERMES is substantially improving the precision of data on semi-inclusive processes because of the experimental advantages mentioned above. Preliminary results of similar quality for the polarized quark distributions have already been released, from an analysis of only the 1995 ^{3}He and 1996 proton data. Twice as many proton data exist from the 1997 running, and a similar amount of deuteron data will be acquired in 1998/99. Kaon identification by the new RICH detector will provide flavour-tagging of strange quarks, for example through the identification of $K^-(\bar{u}s)$. Thus

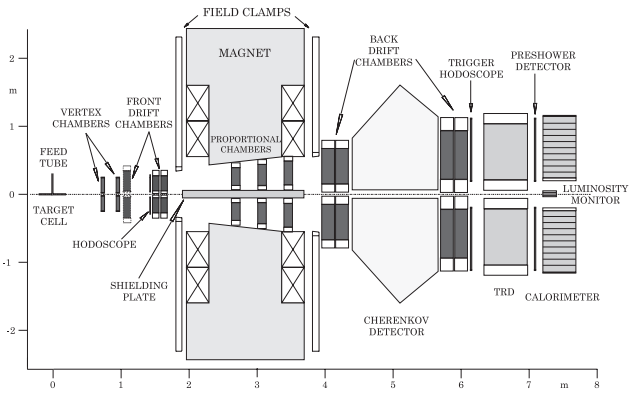

Fig. 19. Schematic side view of HERMES spectrometer.

the full database from HERMES will provide good precision on polarized quark distribution functions. Since precise data from two targets are required to exploit the power of this technique, the definitive HERMES precision will not be available until 2000.

In summary, HERMES will give unique results on semi-inclusive processes while remaining competitive for measurements of $g_1(x)$.

Canadian contribution to the experiment

Discrimination between $e^{\pm}$ and hadrons is provided by the combination of a transition radiation detector (TRD) and electromagnetic shower counters. The Canadian group took the responsibility for the design and construction of the TRD, together with its complex xenon gas recirculation system, relying heavily on the expertise and infrastructure at TRIUMF. The Canadian group has also played a central role in the design and management of the rest of the experiment, including the design of all the wire chambers as well as the design and commissioning of the electron polarimeter at HERA. The demonstration of a high degree of beam polarization ($> 40\%$) was a pre-requisite for the approval of the experiment by DESY.

The experiment was commissioned in the spring/summer of 1995. Data were taken in 1995 on a ^{3}He target and in 1996–97 on H. A few weeks were also spent on high luminosity running with unpolarized targets. The TRD has worked very well over the first three years of operation. The design goal was to provide a pion rejection factor of 100 at 5 GeV with a $e^{\pm}$ efficiency of 90% (PRF= total # of pions/hadrons divided by the # of misidentified pions/hadrons). This was achieved quasi-on-line early in the 1995 run, with typical PRFs of 120 integrated over all energies. Improvements to the interpretation of the TRD data using a probability-based analysis have increased the PRF by a factor of up to 10. More details on TRD performance can be found in [HERMES collaboration, *op. cit.*; R. Kaiser (for the PID group), *Particle identification at HERMES*, HERMES internal note 97-025], and in last year's Annual Report.

The TRIUMF group is also responsible for PID (particle identification) algorithms. Progress was made this year on improving the description of the detector responses (parent distributions) used in the probability analysis of the PID detectors. This work is the basis for the technical portion of the thesis of Mr. J. Wendland (SFU) and is the subject of a HERMES internal note which will be submitted early in 1999 [Wendland, *A new simple Monte Carlo for PID analysis*, Simon Fraser University].

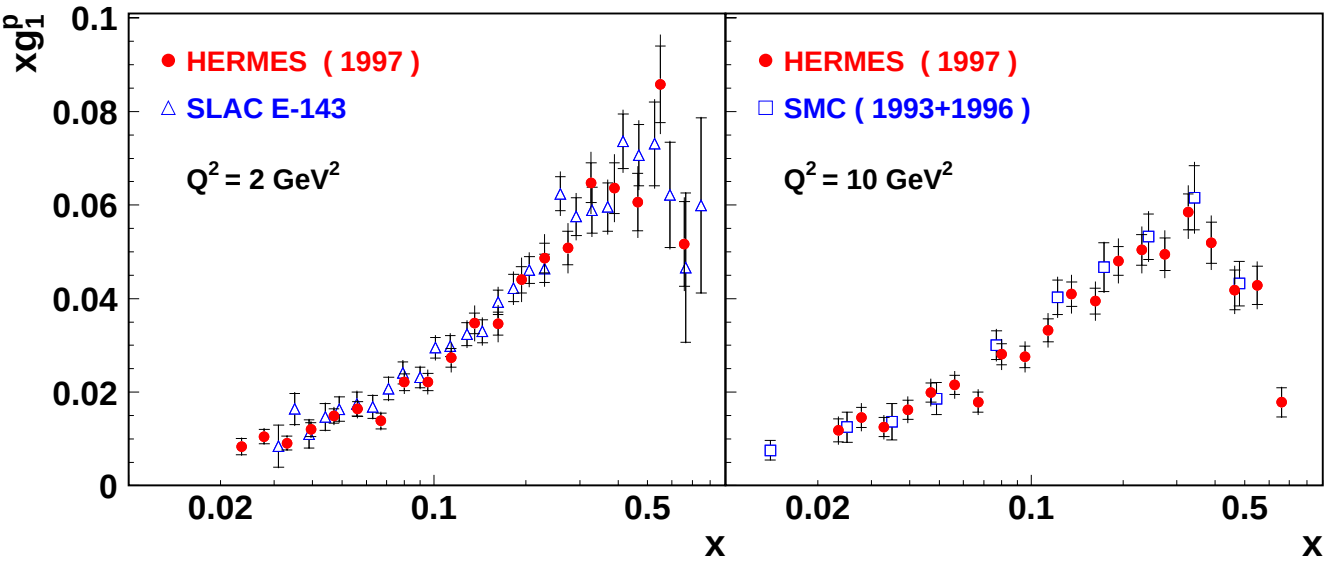

Fig. 20. The spin structure function $g_1^p(x)$ of the proton, multiplied by x, as a function of x. The HERMES data are evolved to a) $Q_0^2 = 2$ GeV^2 and b) $Q_0^2 = 10$ GeV^2, assuming g_1^p/F_1^p to be independent of Q^2. This measurement is compared to recent results for $Q^2 > 1$ GeV^2 from E-143 and from SMC, the latter for $x > 0.011$ only. The error bars show both statistical and systematic contributions.

Physics results

Inclusive scattering and spin structure functions

The spin structure function $g_1(x)$ can be determined from data on the deep inelastic scattering of longitudinally polarized leptons from polarized nucleon targets. The integral of g_1 is a measure of the contribution of the quark spins to the nucleon spin. Results for $g_1^n(x)$ from the 1995 data set on ^{3}He have been published [HERMES collaboration, Phys. Lett. **B404**, 383 (1997)] and formed the basis for the Ph.D. thesis of a Canadian student (R. Kaiser, SFU). However, given that 1995 was a commissioning year, the number of events collected does not represent the full data set on the neutron which will be accummulated by HERMES. On the other hand, the final results for $g_1^p(x)$ from the 1997 data set are at least as precise as any published data. They have now been published [HERMES collaboration, Phys. Lett. **B442**, 484 (1998), hep-ex/9807015] and are shown in Fig. 20, compared to results from SLAC-E143 and SMC at the appropriate Q^2. It is clear that the systematic uncertainties are very well understood in all these experiments, which are based on quite different techniques.

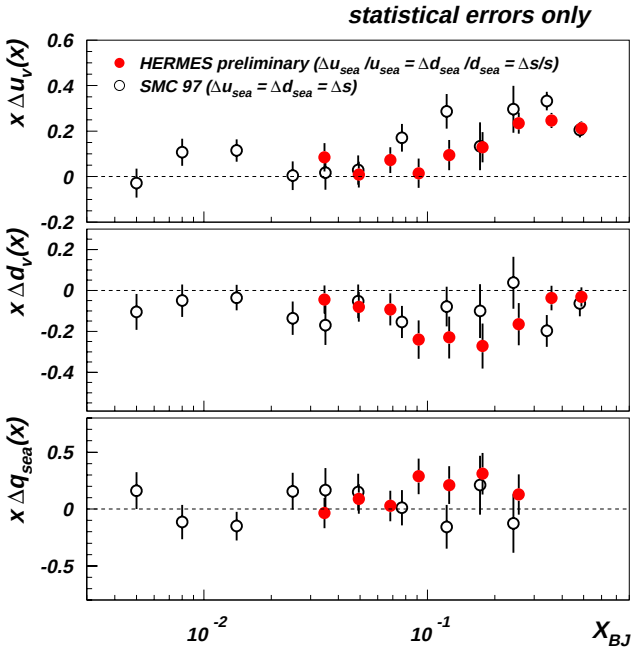

Fig. 21. Preliminary results from 1995/96 for the quark spin distributions of the valence $x\Delta u_v, x\Delta d_v$ and the sea $x\Delta q_{sea}$ as a function of x, and at the measured Q^2 values. They are compared to the results from SMC at a Q^2 of 10 GeV^2.

Semi-inclusive scattering and polarized quark distribution functions

In parallel with the inclusive measurements, HERMES has been designed to measure polarized semi-inclusive DIS. This unique data set (with identified π's and K's) will significantly improve the determination of the individual spin-dependent quark distribution functions. Figure 21 shows that the preliminary results for the polarized quark distributions, based on only undifferentiated hadrons in the 1995 ^{3}He and the 1996 proton data sets, are already competitive with the only previous information on these quantities. A paper based on the full H data set (1996-97) and the 1995 ^{3}He data is in the final stages of preparation.

Physics with unpolarized targets

Although HERMES is primarily a *polarized* deep inelastic scattering experiment, data on *unpolarized* DIS are also taken during short dedicated runs when the density of the target is increased significantly for H_2, D_2, ^{3}He, and N_2. These measurements provide good statistics on processes which do not require polarization (fragmentation functions, light quark sea asymmetry, ρ-meson production, etc.). Some of these processes have been well studied in previous experiments and can be used as consistency checks of the HERMES apparatus and analysis chain. Beyond providing these checks, the unpolarized data set can be used to determine quantities of great current interest such as the flavour asymmetry in the light quark sea. Measurements by NMC at CERN have shown that the Gottfried sum rule is violated significantly. This can be explained as an excess of $d\bar{d}$ pairs over $u\bar{u}$ pairs in the proton. HERMES unpolarized data are sensitive to this asymmetry through a particular combination of observables in hadron production. Results for the ratio $(\bar{d}(x) - \bar{u}(x))/(u(x) - d(x))$ are shown in Fig. 22 and have been published [HERMES collaboration, Phys. Rev. Lett. **81**, 5519 (1998), hep-ex/9807013]. This quantity is clearly nonzero and positive showing that there are indeed more $d\bar{d}$ pairs in the proton sea than $u\bar{u}$ pairs. Note that these E866 results are derived from data on $\bar{d}/\bar{u}$. E866 and HERMES provide complementary data on $\bar{d}/\bar{u}$ and $\bar{d} - \bar{u}$ respectively.

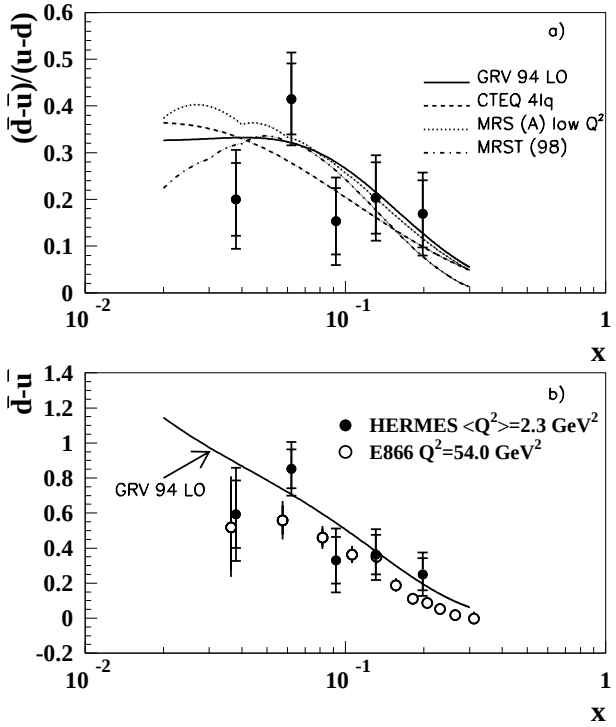

Fig. 22. (a) $(\overline{d} - \overline{u})/(u - d)$ as a function of x. Also included are the GRV 94 LO, CTEQ 4lq, MRS (A) low Q^2, and MRST (98), parameterizations calculated at the appropriate Q^2 for each x-bin. (b) $\overline{d} - \overline{u}$ as a function of x. The curve is the GRV 94 LO parameterization. The open circles represent the E866 determination of $\overline{d} - \overline{u}$ using the Drell-Yan process. The inner error bars represent the statistical uncertainty while the total error bars represent statistical and systematic uncertainties added in quadrature.

ρ meson production

Data on ρ-meson production can be used to study diffractive processes, in particular the spin characteristics of this interaction. Data with very high statistics have been taken on ^{3}He. The angular distribution of the pions from ρ decay can be analyzed to yield the spin density matrix of the ρ, and hence its coupling to that of the virtual photon. The quantity r_{00}^{04} is a measure of the longitudinal polarization of the ρ and varies with Q^2. It is directly related to the ratio $R \equiv \sigma_L/\sigma_T$ of longitudinal to transverse photon cross sections, which is shown as a function of Q^2 in Fig. 23. The HERMES results are the most precise in the lower energy range, and lend support to the previous hypothesis that R is dependent on energy as well as Q^2.

ρ-meson production can also be used to probe the space-time evolution of a virtual quantum state – the quark-antiquark pair $(q\bar{q})$ fluctuation of a photon – by studying its propagation through a perturbing medium. The kinematics of the scattering can be adjusted to vary the *coherence length* l_c, the distance travelled by the off-shell $q\bar{q}$ pair during which it is vulnerable to hard interactions inside the nucleon, and both the *size* and the *expansion time* of the point-like configuration after it has been put on-shell by the Pomeron. By varying the energy ν of the virtual photon, HERMES is able to separate these two effects, since $l_c = 2\nu/(Q^2 + M_{q\bar{q}}^2)$, while the expansion time during which the size and hence the final state

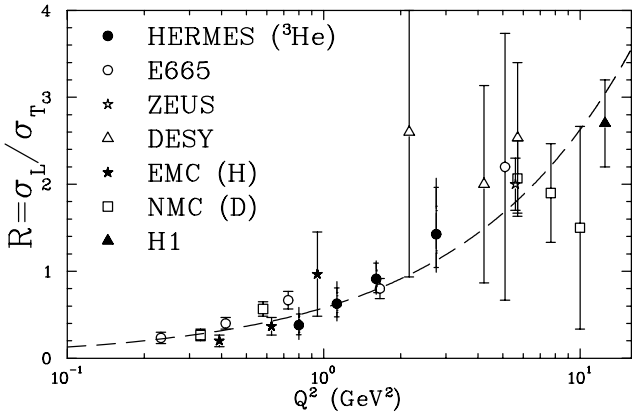

Fig. 23. The ratio $R \equiv \sigma_L/\sigma_T$ of longitudinal to transverse photon cross sections as a function of Q^2, compared to previous data. The dashed line represents a simultaneous power-law fit to all data.

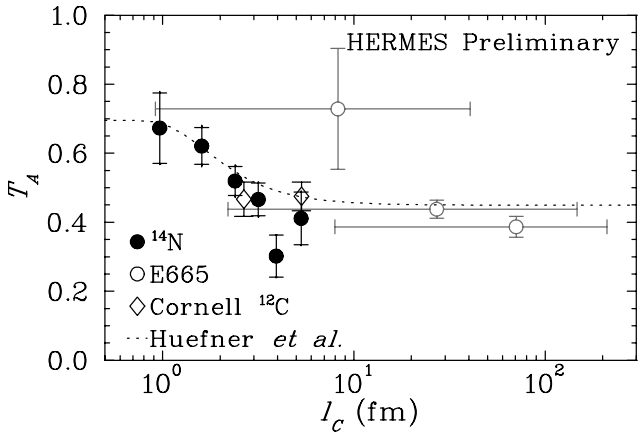

Fig. 24. Nuclear transparency T_A – the ratio of the measured cross section per nucleon in the medium of the nucleus A to that in the nucleon where initial and final state interactions are assumed to be minimal, as a function of coherence length l_c. The HERMES data are for the ^{14}N nucleus, for which the 6% systematic uncertainty in the overall normalization is not shown. The curve is a Glauber calculation. Also shown are previous photoproduction (open diamonds) and muoproduction (open circle) results.

interaction probability remains small is proportional to ν. (The size depends inversely on Q^2, the negative mass squared of the virtual photon, leading to a similar Q^2 dependence of both initial and final state interactions.) Figure 24 shows the first explicit demonstration that the interactions of the photon with the nuclear medium depends on the propagation distance l_c of the $q\bar{q}$ pair. These results have been submitted for publication [HERMES collaboration, hep-ex/9811011].

Fragmentation functions

The Canadian group is also analyzing the unpolarized semi-inclusive data to extract the fragmentation functions (D_q^h), which represent the probability that a quark of flavour q will produce a hadron of type h. These functions are not only interesting in their own right, but are crucial input to semi-inclusive analyses at HERMES. Preliminary results for the so-called favoured (e.g $D_u^{\pi^+}$, $D_d^{\pi^-}$, ...) and disfavoured (e.g $D_u^{\pi^-}$, $D_d^{\pi^+}$, ...) fragmentation functions are shown in Fig. 25 where they are compared to previous measurements by EMC. The fact that there is reasonable agreement between the two experiments, done at very different energies, is further proof that the HERMES semi-inclusive data at relatively low energy can be interpreted in a straightforward manner. In more formal terms, factorization of the hard scattering process $(\gamma^* - q)$ and the subsequent hadronization process is valid. Furthermore, this shows that it is possible to separate the so-called current fragments (coming from the struck quark) from the target fragments (coming from the spectator quarks) for HERMES kinematics.

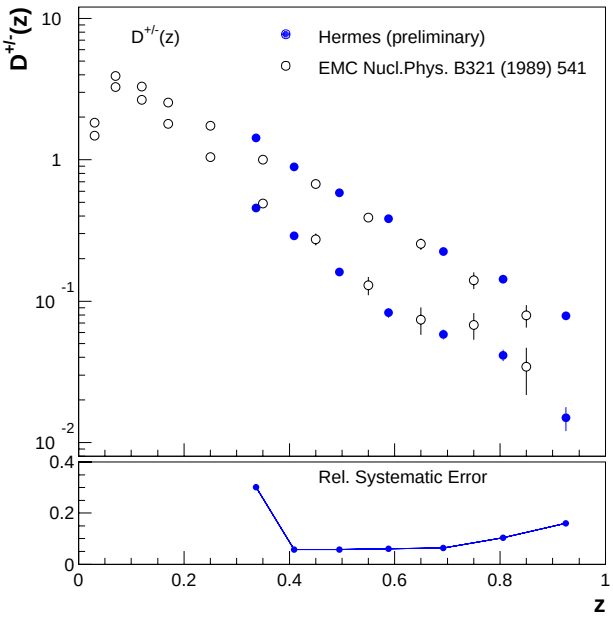

Fig. 25. Favoured (D^+; upper set of points) and disfavoured (D^-; lower set of points) fragmentation functions from HERMES data compared to results from EMC. The latter have been evolved to the HERMES Q^2 of 2.3 GeV^2.

Outlook

The HERMES collaboration has undertaken several upgrades to the spectrometer and the targets: upgrade of the Čerenkov detector to a RICH for kaon identification giving access to the strange sea, the addition of a muon filter wall and improved acceptance to increase our sample of J/ψ's through the detection of the $\mu^+\mu^-$ decay channel, a *forward quadrupole spectrometer* (FQS) to detect the scattered $e^\pm$ at very small angles and thus tag the energy of 'real' photons producing vector mesons such as the J/ψ and ϕ, a silicon tracker in the target chamber mostly to improve the acceptance for Λ particles, and an improved rf dissociator for the atomic beam source which will provide increased target thickness. The RICH and muon filter wall are now operational for 1998 running, and FQS and silicon detector prototypes are installed and under test. A Canadian (A. Miller) is spearheading the development of the FQS. All these upgrades will result in enhanced productivity as the polarized program continues for a few more years, starting with the polarized deuterium target in 1998–99.

Search for T violation in $K_{\mu 3}$ decay
KEK Expt. 246 (Japan-Russia-Canada-Korea-U.S.A. collaboration)

(M.D. Hasinoff, UBC; J.A. Macdonald, TRIUMF; B. Shin, Saskatchewan)

A search for transverse polarization (P_T) of muons in $K^+ \to \pi^0\mu^+\nu_\mu$ ($K^+_{\mu 3}$) decay at the $\sim 10^{-3}$ level is being carried out at the High Energy Accelerator

Research Organization (KEK) in Japan by a collaboration from Canada, Japan, Korea, Russia and the U.S.A. For a weak interaction in the absence of electromagnetic final state interactions, such a component of the muon polarization normal to the decay plane would be an indication of the violation of time-reversal invariance. A feature of P_T in $K_{\mu 3}$ decay is that it does not have contributions from the standard model and consequently, this measurement has the potential to reveal new CP violation physics, given CPT invariance. Motivation to search for additional sources of CP violation arises from the observed baryon asymmetry in the universe, which cannot be explained by the CP violation in the standard model alone. Furthermore, recent theoretical progress of electroweak baryogenesis suggests that new CP violation sources might exist at the electroweak scale which can be accessible experimentally.

In $K^+_{\mu 3}$ decay, the hadronic matrix element can be described as

$$< \pi|J|K >= f_+^K(q^2)(\tilde{p}_K + \tilde{p}_\pi) + f_-^K(q^2)(\tilde{p}_K - \tilde{p}_\pi)$$

where $\tilde{p}_K$ and $\tilde{p}_\pi$ are the four momenta of the kaon and pion, respectively. $f_+^K(q^2)$ and $f_-^K(q^2)$ are the form factors of the hadronic matrix elements as a function of momentum transfer squared (q^2). Time-reversal invariance requires that the phases of f_+^K and f_-^K are relatively the same; in other words, if the parameter $\xi(q^2) \equiv f_-^K(q^2)/f_+^K(q^2)$ is defined, ξ should be a real number. Conversely, a non-zero value of Imξ would indicate T violation.

The experiment is being carried out at the low energy kaon beam line (K5) of the KEK 12 GeV Proton Synchrotron (PS) and has been described in previous Annual Reports. Briefly, the technique uses stopped kaons in conjunction with a 12-gap superconducting toroidal spectrometer, a finely segmented CsI photon calorimeter, and a muon polarimeter capable of a measurement with low backgrounds and small systematic errors at the 10^{-3} level for ΔP_T.

P_T of the muons stopped in the polarimeter manifests itself as either a clockwise (cw) or counter clockwise (ccw) asymmetry in the decay positron distribution, depending on the emission angle of the pion relative to the beam axis. By summing over the 12 spectrometer gaps, several systematics, such as the effect of an asymmetric kaon stopping distribution in the target and unequal detection efficiency of positron counting, can be cancelled. Moreover, by taking the double ratio for events with the π^0 going into the forward and the backward directions, further cancellation of systematic errors is possible because our experiment uses stopped kaons.

Good $K_{\mu 3}$ events are selected by cutting on the muon momentum and mass (from time of flight), on the π^0 invariant mass spectrum from photon total energy and direction in the calorimeter, and on the kaon decay time spectrum. A kinematic cut on the opening angle between the muon and the pion is very useful for rejecting any $K_{\pi 2}$ pions remaining after the momentum cut. Finally, the missing-mass cut is tuned to reject events from kaon decay-in-flight. The clean π^0 events consist of 2-photons in the CsI. In order to recover some of the π^0 acceptance lost due to the "muon" holes in the CsI array, we also accept events with only 1-photon cluster satisfying a high energy threshold (70 MeV), for which most of the π^0 kinematic information is preserved.

By June we accumulated a total of 3.6 million events in the π^0-forward and π^0-backward regions. We are performing two independent analyses in the group in order to check consistency and estimate systematic errors associated with the analysis. The major differences in the two analyses lie in the charged particle tracking algorithm and in the photon clustering algorithm in the CsI(Tl) array. The near equivalence of the two analyses was checked by comparing good final events in both analyses and their correlations. However, some fraction of the good events are uncommon and the difference between their central values is attributed to the statistical fluctuations of this part. Both analyses have finished processing all the 1996 and 1997 data. The two results are consistent with null T violation within the statistical error,

$$P_T = (-2.55 \pm 5.68) \times 10^{-3},\ \mathrm{Im}\xi = (-0.77 \pm 1.86) \times 10^{-2}$$

for one analysis, and

$$P_T = (-0.25 \pm 5.72) \times 10^{-3},\ \mathrm{Im}\xi = (-0.01 \pm 1.80) \times 10^{-2}$$

for the other. We are currently engaged in a discussion how best to combine these two results. When the 1998 data have been analyzed, a statistical limit of $\Delta \mathrm{Im}\xi = 0.01$ is expected.

Because the result from existing data will be statistics limited, KEK E246 will benefit from further data-taking and has been granted 200 shifts of additional beam time starting in the fall of 1999.

Measurement of the flavour singlet form factors of the proton
TJNAF Experiment E91-017
(W.T.H. van Oers, Manitoba)

The structure of the nucleon at low energies in terms of the quark and gluon degrees of freedom is not well understood. The $G0$ experiment is to measure two proton ground state matrix elements which are sensitive to point-like strange quarks and hence to the quark-antiquark sea in the proton. The matrix elements of interest are the elastic scattering vector

weak neutral current 'charge' and 'magnetic' form factors, G_E^Z and G_M^Z, respectively. These can be extracted from a set of parity violating electron-proton scattering measurements. If one assumes a relationship between the proton and neutron structure in that the proton and neutron differ only by the interchange of up and down quarks, i.e., isospin symmetry, the strange quark (as well as the up and down quark) contribution to the charge and magnetic form factors of the nucleon can be determined. This would result from taking appropriate linear combinations of the weak neutral form factors and their electromagnetic counterparts.

Determinations of both the charge and magnetic strange quark form factors are of fundamental interest, as they would constitute the first direct evidence of the quark sea in low energy observables. The objective of the $G0$ experiment is to determine these contributions to the proton form factors at the few percent level. Observations at high energy suggest that the strange quarks carry about 1/2 as much momentum as up and down quarks in the sea. It is important to determine both the role of the quark sea and the relevance of strange quarks at low energy where there are voids in understanding the theory of the strong interaction (quantum chromodynamics, QCD). Even if the strange quark contributions do not amount to the level of sensitivity of the experiment, upper limit determinations at this level are as valuable as non-zero results. The matrix elements, G_E^Z and G_M^Z, are also relevant to discussions of the Ellis-Jaffe sum rule and the pion-nucleon sigma term; there is uncertainty in both of these about the strange quark contributions. The $G0$ experiment will allow the determination of the strange quark contributions to the proton charge and magnetic form factors in a much more straightforward manner than is possible with regard to the corresponding observables in the above two determinations.

In the $G0$ experiment parity violating longitudinal analyzing powers will be measured in electron-proton scattering in the range $0.1 \leq Q^2 \leq 1.0$ GeV^2 at both forward and backward angles. The longitudinal analyzing power is defined as

$$A_z = \frac{1}{P}\,[\sigma^+(\theta) - \sigma^-(\theta)]/[\sigma^+(\theta) + \sigma^-(\theta)]\ ,$$

with P the polarization of the incident electron beam and the $+$ and $-$ signs indicating the helicity state. Making pairs of measurements at forward and backward angles will allow the separation of G_E^Z and G_M^Z. Predicted longitudinal analyzing powers range from about $(-3$ to $35)\ \times 10^{-6}$; it is planned to measure the longitudinal analyzing powers with statistical uncertainties of $\Delta A/A = 5\%$ and systematic uncertainties related to helicity correlated effects of $\Delta A/A \leq 2.5 \times 10^{-7}$. In the first phase of the experiment longitudinal analyzing powers will be measured concurrently at seven values of the momentum transfer in the range $0.1 \leq Q^2 \leq 1.0$ GeV^2. With an electron beam polarization of 0.49, the time required to reach this precision in the first phase measurement will be about 700 hours. It now appears highly probable that by the time of data-taking for the $G0$ experiment higher beam polarizations will have been reached, reducing the data-taking time by close to a factor of two. However, it must be realized that it is not the actual data-taking time that governs the length of the experiment but rather making elaborate control measurements to determine the corrections that have to be made to the measured asymmetries and to understand systematic errors. Using the result for G_M^Z at $Q^2 = 0.1$ GeV^2 from the SAMPLE experiment now being performed at the MIT-Bates Laboratory, it would be possible to separate the charge and magnetic form factors at the lowest Q^2 bin after the first phase measurement. In the second phase experiment each subsequent backward angle analyzing power measurement would require from 0.5 to 1 month of running time. It should be noted that the overall uncertainties of a few times 10^{-8} quoted for the recent parity violation experiments at PSI and the University of Bonn and quoted for the systematic uncertainties in the parity violation experiments at MIT-Bates and Mainz suggest that systematic uncertainties of a few times 10^{-7} should be attainable in the $G0$ experiment. The preliminary result of the HAPPEX experiment shows that there exists no barrier at Jefferson Lab to successfully perform the $G0$ experiment.

The *G0* collaboration

The $G0$ experiment will be carried out by a collaboration of scientists from Canada, France, and the United States, with funding provided through NSERC (Canada), IN2P3 (France), and DOE/NSF (US).

The experiment underwent a Cost and Schedule Review in February, and the conclusions of the Review Committee included a very strong statement in support of the experiment, as well as recommendations for an updated budget, schedule, and implementation of a Project Management Plan. In early spring, both the Canadian and French subgroups of the collaboration received notification of the successful outcomes of their funding requests. Over the course of the spring and summer, much effort was put into developing and finalizing the $G0$ Management Plan. This Management Plan was submitted to the US DOE and NSF agencies in late summer, and the updated funding level and profile was successfully defended and accepted.

Canadian contribution to the *G*0 experiment

The Canadian members of the *G*0 collaboration, based at the universities of Manitoba, Northern British Columbia, and at TRIUMF, have been asked to : (i) develop and produce specialized photomultiplier tube bases for the main detector arrays; (ii) machine and produce the cryostat-exit detector arrays for the backward angle measurements; (iii) develop and test specialized beam monitors, control apparatus, and "parity" type electronics to read out these monitors; and (iv) design, build and test an automated magnetic field measuring apparatus complete with its own data acquisition system.

This past year has seen much progress in the designing and building of many of the various components/subsystems listed above.

The *G*0 main detector array

The heart of the *G*0 detection system is a spectrometer which consists of an 8 sector toroidal magnet, with an array of scintillation detectors located at the focal surface of each sector (see Fig. 26). Due to geometry, resolution, and rates considerations, the shapes of both the prototype scintillators and their associated lightguides have become quite elaborate. Since data will not be acquired in event-by-event mode in this experiment, and since the scintillator arrays are the only detectors to measure the scattered particles in the forward angle mode, the performance of these focal-plane detectors (FPD) are of critical importance. The timing and pulse shape characteristics of this system must be fine-tuned at the hardware level because it will not be possible to reconstruct individual events. Furthermore, the "real signal" rates associated with many of the FPD segments will be quite high (1 MHz) and the photon yields may be quite large. As such, special demands will be made on the photomultiplier tubes (PMT) and especially on their associated divider/base circuit.

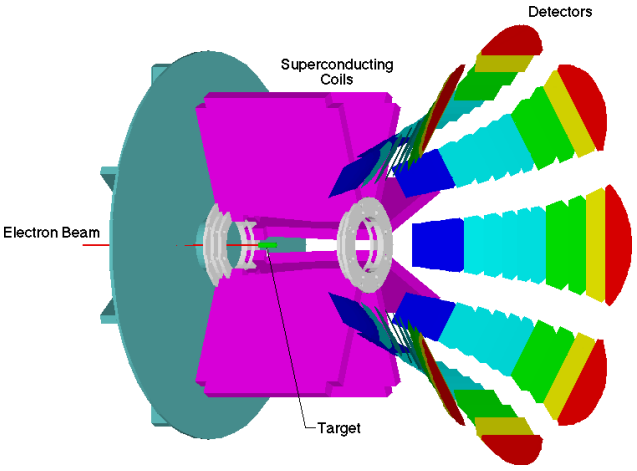

Fig. 26. View of the *G*0 superconducting toroidal spectrometer with one sector and the spectrometer housing removed.

Much progress has been made in the design, development, and building of the *G*0 bases at TRIUMF. In 1997, 4 prototype "high-rates" bases were constructed and delivered to TJNAF for tests. Based on these studies, modifications were made and a second set of prototype bases were constructed and delivered to TJNAF in early 1998. In the early summer, 12 final prototype bases were constructed and delivered to TJNAF to be used in conjunction with the first set of prototype focal-plane detectors, and fabrication of the actual "production" bases began in earnest. With the help of summer students (funded partly through the TRIUMF Summer/Co-op Students program and partly through the *G*0 NSERC grant), the assembling of the electrical components for all of the production bases has been completed. The remaining tasks for this subsystem are related to the fabrication and assembly of the mechanical housing for the PMT and base.

As well, the Canadian subgroup is responsible for the testing and characterizing of all of the photomultiplier tubes to be used with the TRIUMF/*G*0 high-rates bases. With the help of summer students at TJNAF, the primary testing and characterization of the PMTs was completed in late summer.

The cryostat-exit detector array

For the backward angle measurements, simulation results indicate that the elastic and inelastic electrons could be more cleanly separated with the addition of a second array of scintillation detectors, located near the spectrometer-cryostat exit-windows. The geometry of these cryostat-exit detector (CED) arrays is still being studied at present. Due to the resident expertise at TRIUMF in producing high quality scintillation detectors and lightguides, the Canadian subgroup has been asked to play a main role in the prototyping and production of the CEDs. Once the preliminary shapes have been optimized, it is expected that several prototypes will be produced at TRIUMF and delivered to TJNAF or Louisiana Tech for further studies. Full scale production of the CEDs would then follow shortly after these studies are completed. The CEDs will also make use of the same types of photomultiplier tubes and specialized TRIUMF/*G*0 bases as the focal-plane detectors.

Resonant cavity position and current monitors

Five sets of "XYQ" monitors will be required in order to measure the beam current (charge) and trajectory (positions and angles) at several critical locations (directly upstream of the target, at an upstream dispersed focus, and further upstream in the beam line). The proposed current monitor will be of the resonant

cavity type. Presently, the design consists of a cylindrical cavity operating in the TM010 mode at 1497 MHz. A beam current sensitivity of $\pm 4 \times 10^{-5}$ measured in a 33 ms integration-time sample will be required to monitor and correct for possible helicity correlated intensity modulations. For the beam position monitors (BPM), there are two designs under consideration. The presently existing BPMs consist of stripline monitors operating in a special "switched electrode electronics" (SEE) mode. An alternate proposal involves the use of a pair of cylindrical resonant cavities (X and Y) operating in the TM110 mode. In either case, a spatial resolution of better than 25 μm at an integration time of 33 ms will be required.

The beam current and the stripline position monitors were tested during an engineering run in July, 1997 at TJNAF. The run was organized by members of the *G*0 Canadian subgroup and personnel from TJNAF (Hall C), with much of the readout electronics provided by the Canadian subgroup. Precision analog subtractor/divider modules and voltage-to-frequency converters from the TRIUMF parity experiment were readily adapted to the TJNAF beam monitors. Helicity correlated properties of the TJNAF polarized electron beam and noise characteristics of some of the beam monitors were successfully measured. Analysis of the data indicates that the beam current monitors will meet the specification requirements of $\Delta Q/Q \leq 4 \times 10^{-5}$ (in 33 ms). The stripline SEE monitors were able to provide position determinations with $\Delta X \leq 1$ μm (in 33 ms), which will also meet the specification requirements. Further test-beam time is planned for the future.

To read out the analog signals from the various beam current and position monitors, and to provide feedback control signals, specialized parity type electronics will be required for the *G*0 experiment. Much of this electronics, such as precision analog subtractors/dividers and precision voltage-to-frequency converters, has already been designed and used by members of the Canadian subgroup in their parity experiments at TRIUMF. Modifications, driven by the requirements of the *G*0 experiment, were made to some of these electronics modules and they were operated successfully at the July, 1997 engineering run at TJNAF, as mentioned above. Since that time, several voltage-to-frequency converters of the TRIUMF/parity variety have been requested by TJNAF for the *G*0 experiment. Construction of these 32-channel precision V-to-Fs was completed at TRIUMF and delivery was made to TJNAF in early 1998.

Magnetic field measuring apparatus

An automated field measuring apparatus will be used to provide a magnetic verification of the *G*0 superconducting toroid by measuring the zero-crossing locations of specific field components at selected points of symmetry. This will be carried out by scanning a predefined set of "contour" lines, and determining where specific field components reverse signs. The system must be capable of providing a position determination of 0.2 mm and a field determination of 0.2 G. A partially-automated carriage will be used in conjunction with precision hall probes to meet these requirements.

The present design concept is illustrated in Fig. 27. Here, the magnetic verification device will consist of a small carriage which mounts to the spectrometer cryostat and can be rotated from sector to sector. Located on the carriage will be a movable magnetic field probe, positioned via a high-precision position or shaft encoder. The mapping of the zero-crossing points will be carried sector by sector, and the field data will be acquired via a precision DVM and a GPIB/PC-based data acquisition system. This first order conceptual design for the field measuring apparatus is presently being completed.

Canadian subgroup of the *G*0 collaboration: J. Birchall, W.R. Falk, L. Lee, S.A. Page, W.D. Ramsay, W.T.H. van Oers, R.J. Woo (Manitoba); E. Korkmaz, G. O'Reilly (University of Northern British Columbia); C.A. Davis (TRIUMF).

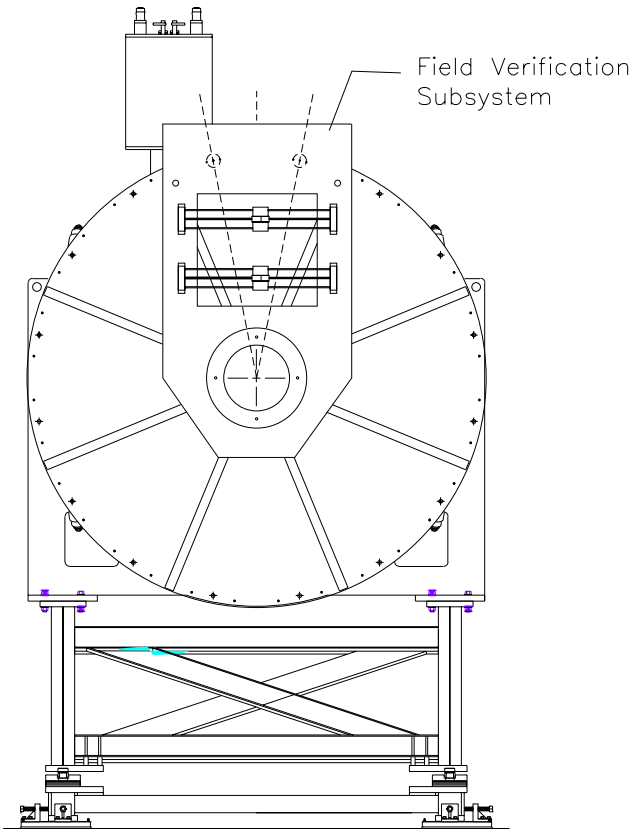

Fig. 27. Schematic layout of the magnetic verification apparatus, mounted to the spectrometer cryostat.